Journal Pre-proofs

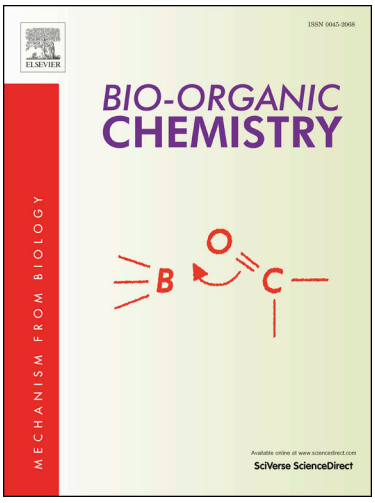

Design and synthesis of new 1,6-dihydropyrimidin-2-thio derivatives targeting VEGFR-2: molecular docking and antiproliferative evaluation

Adel A. Marzouk, Salah A. Abdel-Aziz, Kamal S. Abdelrahman, Amira S. Wanas, Ahmed M. Gouda, Bahaa G.M. Youssif, Mohamed Abdel-Aziz

PII: S0045-2068(20)31387-0
DOI: https://doi.org/10.1016/j.bioorg.2020.104090
Reference: YBIOO 104090

To appear in: *Bioorganic Chemistry*

Received Date: 6 April 2020
Revised Date: 16 June 2020
Accepted Date: 7 July 2020

Please cite this article as: A.A. Marzouk, S.A. Abdel-Aziz, K.S. Abdelrahman, A.S. Wanas, A.M. Gouda, B.G.M. Youssif, M. Abdel-Aziz, Design and synthesis of new 1,6-dihydropyrimidin-2-thio derivatives targeting VEGFR-2: molecular docking and antiproliferative evaluation, *Bioorganic Chemistry* (2020), doi: https://doi.org/10.1016/j.bioorg.2020.104090

Design and synthesis of new 1,6-dihydropyrimidin-2-thio derivatives targeting VEGFR-2: molecular docking and antiproliferative evaluation

Adel A. Marzouk [a], Salah A. Abdel-Aziz [a,b], Kamal S. Abdelrahman [a], Amira S. Wanas [c,d], Ahmed M. Gouda [e], Bahaa G. M. Youssif [f], Mohamed Abdel-Aziz [g]

[a]Department of Pharmaceutical Chemistry, Faculty of Pharmacy, Al-Azhar University, Assiut Branch, Assiut-71524, Egypt; [b]Department of Pharmaceutical Chemistry, Faculty of Pharmacy, Deraya University, Minia, Egypt; [c] National Center for Natural Products Research, University of Mississippi, MS 38677, USA; [d] Pharmacognosy Department, Faculty of Pharmacy, Minia University, 61519-Minia, Egypt; [e] Department of Medicinal Chemistry, Faculty of Pharmacy, Beni-Suef University, Beni-Suef 62514, Egypt; [f] Pharmaceutical Organic Chemistry Department, Faculty of Pharmacy, Assiut University, Assiut 71526, Egypt; [g] Department of Medicinal Chemistry, Faculty of Pharmacy, Minia University, 61519-Minia, Egypt.

Short running title: Novel dihydropyrimidin derivatives as VEGFR-2 inhibitors

******To whom correspondence should be addressed:*

Mohamed Abdel-Aziz, Ph.D. Department of Medicinal Chemistry, Faculty of Pharmacy, Minia University, 61519-Minia, Egypt.

Tel.:(002)-01003311327

E-mail address: Abulnil@hotmail.com

Bahaa G. M. Youssif, Ph.D. Pharmaceutical Organic Chemistry Department, Faculty of Pharmacy, Assiut University, Assiut 71526, Egypt.

Tel.: (002)-01098294419

E-mail address: bgyoussif@ju.edu.sa, bahaa.youssif@pharm.aun.edu.eg

Abstract

A series of new 1,6-dihydropyrimidin-2-thiol derivatives (**scaffold A)** as VEGFR-2 inhibitors has been designed and synthesized. Compounds **3a**, **3b**, **3e** and **4b** have been selected for *in vitro* anticancer screening by the National Cancer Institute. Compound **3e** showed remarkable anticancer activity against most of the cell lines tested, where a complete cell death against leukemia, non-small cell lung cancer, colon, CNS, melanoma, and breast cancer cell lines was observed. *In vitro* five dose tests showed that compound **3e** had high activity against most of the tested cell lines with GI_{50} ranging from 19 to 100 μM and selectivity ratios ranging between 0.75 and 1.71 at the GI_{50} level. VEGFR-2-kinase was tested against **3a**, **3b**, **3e**, **4b** and sorafenib was used as a reference. Compounds **3a** and **3e** were the most potent analogues with IC_{50} values of 386.4 nM and 198.7 nM against VEGFR-2, respectively, in comparison to sorafenib (IC_{50}= 0.17 nM). The results of the docking study showed a good fitting of the new compounds to the active site of VEGFR-2 with binding free energies in the range of -9.80 to -11.25 kcal/mol compared to -12.12 kcal/mol for sorafenib. Compounds **4a-e** with the hydroxyimino group had a higher affinity to VEGFR-2 than their parent derivatives **3a-e**.

Keywords: VEGFR-2, Dihydropyrimidine, Docking, Antiproliferative

Graphical abstract

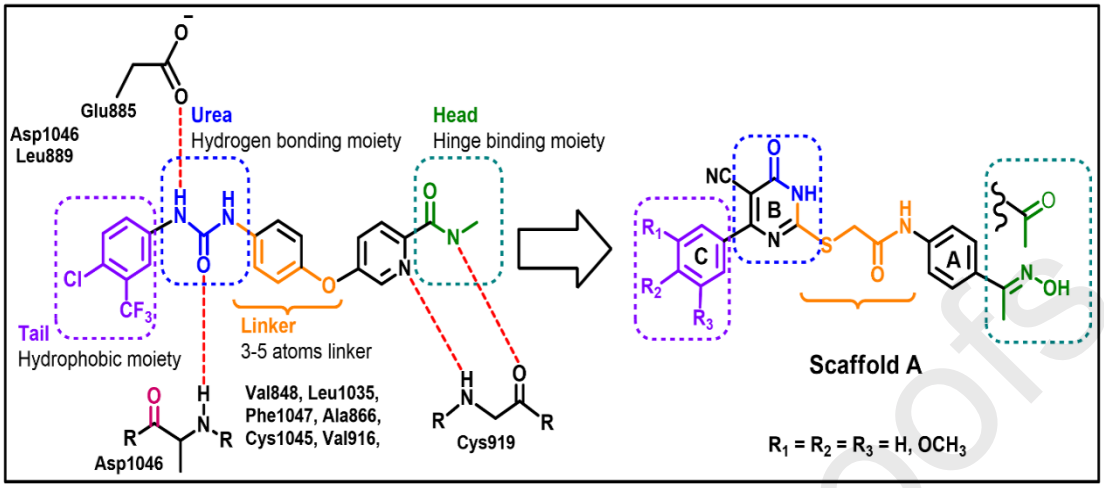

Highlights

- A series of novel 1,6-dihydropyrimidin-2-thio **(3a-e** and **4a-e)** was designed and synthesized.
- Compounds **3a**, **3b**, **3e** and **4b** were selected for *in vitro* anticancer activity by National Cancer Institute.
- Compound **3e** exhibited a remarkable anticancer activity against most of the cell lines tested.
- *In vitro* five dose assay results showed that **3e** have GI_{50} ranging from 19 to 100 μM with selectivity ratios from 0.75 to 1.71.
- Compounds **3a** and **3e,** the most potent analogues against VEGFR-2, showed a good fitting to the active site of VEGFR-2.

1. INTRODUCTION

Cancer is a major global health issue. While progress has been made in the treatment and prevention of cancer, it remains the second biggest cause of death in the world. However, efficacy in cancer treatment remains a concern in the 21st century, and innovative and safer anticancer agents with a wider range of cytotoxicity to tumor cells need to be investigated [1]. Biginelli first reported dihydropyrimidinones (DHPMs) a century ago when the multicomponent reaction was discovered [2]. Dihydropyrimidinone scaffold is a class of highly pharmacologically effective heterocyclic compounds that attract considerable interest. They have a diverse drug profile such as antimicrobials [3], antimalarial [4], antitrypanosomal [5] and anticancer activity [6-8]. Monastrol **I** (**Figure 1**) is one of the tetrahydropyrimidine derivatives that has been established as a new cell permeable molecule that results in mitotic mammalian cell arrest by blocking the bipolar mitotic spindle. [9]. In addition, several diverse dihydropyrimidinones have been synthesized, which show promising antitumor activity, including ethanehydrazonoyl-pyrimidinone **II** [10] (**Figure 1**).

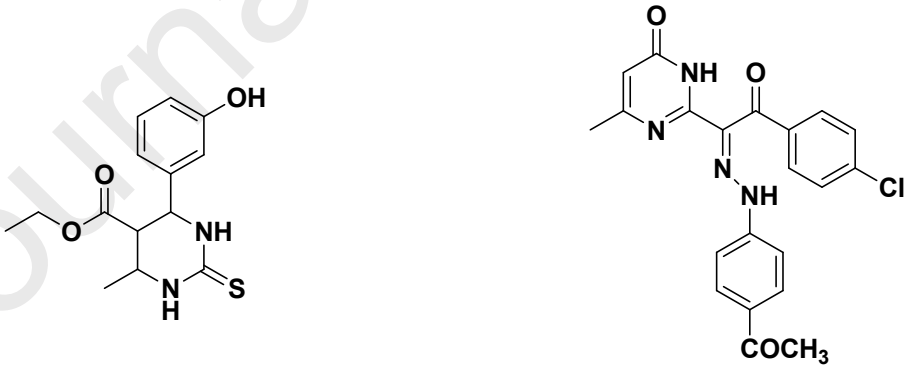

Figure 1: Structure of monastrol **I** and compound **II**

Abnormal angiogenesis plays an important role in cancer and tumor metastases and represents the necessary pathway through which the tumor passes from benign to malignant. Vascular endothelial growth factor receptor-2 (VEGFR-2) is the main and most critical regulator of angiogenic factors associated with tumor angiogenesis [11]. VEGFR-2 can lead to angiogenesis by binding to VEGF leading to stimulation of downstream signaling cascades and certain endothelial reactions, such as increased vessel permeability and increased endothelial cell proliferation. VEGF/ VEGFR-2 blockage therefore offers a promising strategy for anti-angiogenic therapy in the treatment of carcinoma, especially metastatic and progressive solid tumors. [12].

Oxime moiety is distinguished by its simple coordination with metal ions and may participate in hydrogen bonding to the residues of amino acids in the active site of different enzymes. By doing so, the oxime moiety can improve the binding site of the entire molecule [13]. Oximes may also release nitric oxide (NO) free radicals that have a cytostatic and cytotoxic effect on tumor cells. NO can prevent tumor cells from metastasizing and help the macrophage kill tumor cells [14].

Based on the aspects described above and in the continuation of our efforts to discover small molecules with potential anticancer activity [15-19], the objective of this work is to synthesize a hybrid series of dihydropyrimidine derivatives containing oxime as NO release moiety (**Scaffold A)**. This hybridization was intended for synergistic effect, enhancement of anticancer activity and/or decrease of side effects, if any.

1.1. Rational Design

Activation of VEGFR-2 plays an important role in tumor survival, angiogenesis, and migration. Over the last two decades, several potent VEGFR-2 inhibitors have been identified and approved by the FDA for the treatment of different types of cancers. [20-22]. To identify the essential binding interactions involved in inhibition of VEGFR-2, five crystal structures of the enzyme (4ASD, 4AC [22], 3WZD, 3WZD, 3WZE [23], 2RL5 [24]) bound to different inhibitors (sorafenib, lenvatinib, 2RL, and axitinib) were analyzed, **Fig. 2**. Investigation of the binding modes of these inhibitors using discovery studio Visualizer [25] and LigPlot+ [26] revealed the importance of hydrogen bonding interaction with Lys868, Glu885, Cys919, and Asp1046. In addition, the four inhibitors exhibited similar hydrophobic interactions with Val848, Ala866, Leu889, Val916, Leu1035, Cys1045, and Phe1047 amino acids in VEGFR-2 (**Supplementary data, Fig. S1-4**).

The general structure of VEGFR-2 inhibitors consists of four distinct moieties [27]. These moieties include hinge-binding moiety, linker (3-5 atoms), hydrogen bonding moiety (amide/urea) and a hydrophobic tail that occupy the allosteric hydrophobic pocket of the enzyme, **Fig. 2**.

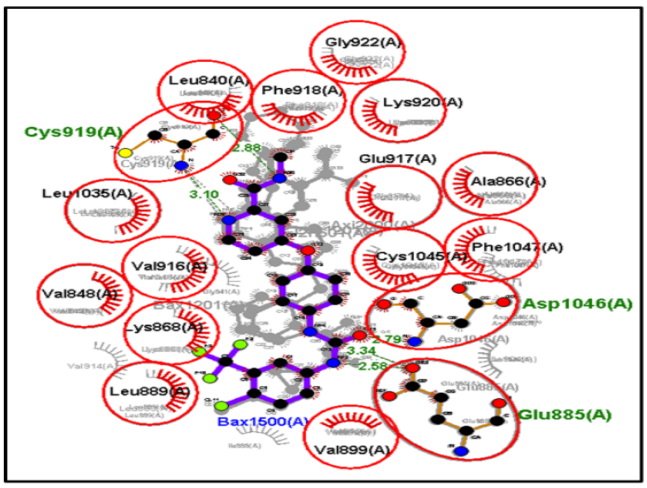

Fig. 2. A superimposition plot of sorafenib, lenvatinib, 2RL, axitinib bound to VEGFR-2 (pdb codes: 4ASD, 4AC, 3WZD, 3WZD, 3WZE, 2RL5), sorafenib is shown in full purple color and is overlaid on lenvatinib, 2RL and axitinib (grey color), red circles and ellipses identify the equivalent residues in the five 3D structures, hydrogen bonding interactions with Lys868, Glu885, Cys919, and Asp1046 shown as olive green dotted line.

In the current study, scaffold **A** (**Fig. 3**) was designed bearing the four pharmacophoric features of VEGFR-2 inhibitors. The acetyl/hydroxyamino head in scaffold **A** was designed to form hydrogen bonding interactions with Cys919. Compared to sorafenib, the linker in scaffold **A** was designed to be more flexible and can interact with VEGFR-2 through both hydrophobic and hydrogen bonding interactions. Moreover, the amide group (hydrogen bonding moiety) was cyclized into a dihydropyrimidine ring (B) which can provide multiple hydrogen bonding interactions with the enzyme. Ring C was also substituted with mono/di/tri-methoxy groups to occupy the allosteric hydrophobic pocket and interact hydrophobically with hydrophobic residues in the enzyme.

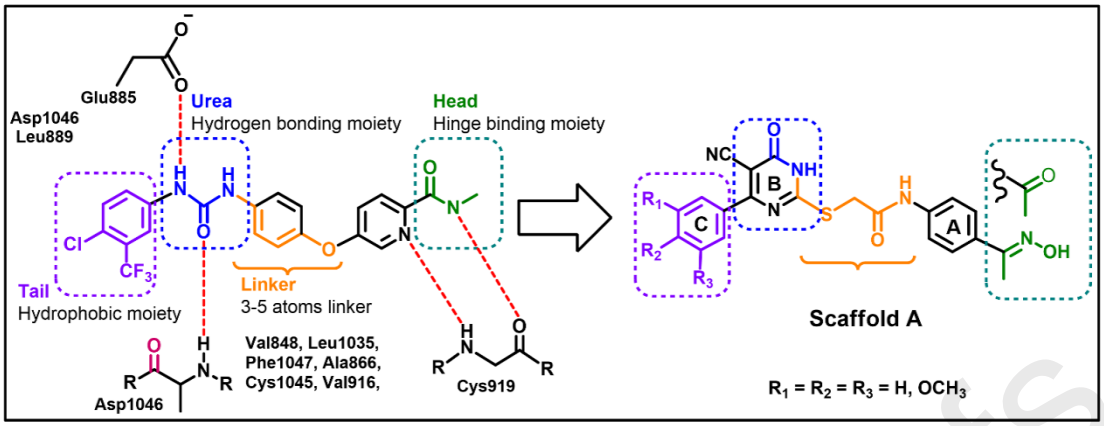

Fig. 3. Rational design of **scaffold A**.

2. RESULTS AND DISCUSSION

2.1. Chemistry

Synthesis of compounds **4a-e** is outlined in **Scheme 1**. Compounds **1a-e** were synthesized by a single pot reaction of benzaldehyde derivatives, ethyl cyanoacetate and thiourea in presence of anhydrous potassium carbonate according to modified Biginelli reaction [28] (**Scheme 1**).

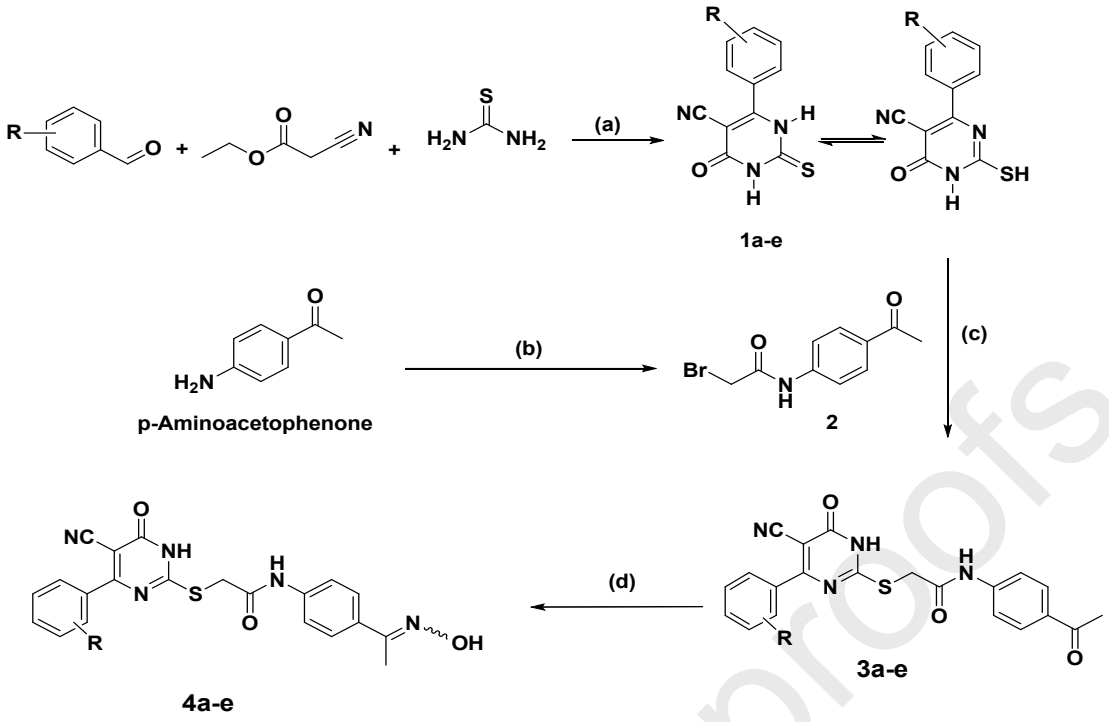

Scheme 1. Synthesis of compounds **3a-e** and **4a-e**

Reagent and reaction conditions: a) K_2CO_3, absolute ethanol; b) bromoacetyl bromide, K_2CO_3, CH_2Cl_2; c) acetone, K_2CO_3; d) Hydroxyl amine hydrochloride, absolute ethanol.

The target compounds **3a-e** were prepared by refluxing compounds **1a-e** with N-(4-acetylphenyl)-2-bromoacetamide **2** in the presence of potassium carbonate for 4-8 h. The structure of **3a-e** was confirmed by IR, ^{1}H NMR, ^{13}C NMR and HRMS (ESI) spectroscopy. The IR spectra of **3a-e** showed significant stretching bands at 3453-3307 cm^{-1} assigned to NH, 2212-2193 cm^{-1} related to (CN), two (C=O) stretching bands appears at 1674-1699 cm^{-1} and 1674-1653 cm^{-1} related to (CO-NH) and (CO-CH_3) respectively. A stretching band at 1653-1592 cm^{-1} related to (C=N) and 1606-1592 cm^{-1} related to (C=C). Compounds **3b-d** showed significant stretching band at 1327-1303 cm^{-1} related to methoxy groups. ^{1}H NMR spectra for compounds **3a-e** showed three singlet peaks at δ 11.17-11.29 ppm related to amidic (NH) proton, at δ 3.8-3.9 ppm related to (S-CH_2) and at δ 2.40-2.50 ppm related to (CO-CH_3).

Moreover, compounds **3b** and **3c** showed singlet peak appeared at δ 3.74-3.75 ppm related to methoxy groups. Furthermore, compound **3d** have tow methoxy groups showed two singlet peaks at δ 3.74 and 3.76 ppm. Moreover, compound **3e** have three methoxy groups showed two singlets for the three methoxy groups at δ 3.76 ppm and at δ 3.69 ppm. ^{13}C NMR spectra of compounds **3a-e** showed characteristic signals at δ 196.50-196.92 ppm (CO-$\underline{C}H_3$) and a signal related to methyl group appeared at δ 26.28-26.75 ppm, (CN) appeared at δ 120.0-120.6 ppm and two signals at δ 166.48-167.60 ppm and at δ 168.25-168.66 ppm related to cyclic amide and aromatic amide, respectively. HRMS **(**ESI**)** data for compounds **3a-e** further confirmed their assigned structures. The m/z value of molecular ion peak [M-H] for each compound was close to the calculated one in all cases.

Oxime derivatives **4a-e** was prepared by heating at reflux a mixture of **3a-e** and hydroxylamine hydrochloride in absolute ethanol. IR spectra of compounds **4a-e** were characterized by the appearance of intense broad bands at 3588-3300 cm^{-1} related to OH and NH groups. In addition to (C=N) and (<u>CO</u>-NH) groups which exhibited stretching vibration at 1671-1619 cm^{-1} and 1650-1687 cm^{-1}, respectively, also the characteristic band of (CN) at 2342-2200 cm^{-1}. ^{1}H NMR spectra for oximes **4a-e** showed the appearance of downfield singlets in the range δ 10.45-10.86 ppm related to the hydroxyl group. The resonances of NH, S-CH_2, and CH_3 protons were observed in the expected regions at δ 11.08-11.2 ppm, δ 3.92-4.21 ppm and δ 2.12-2.14 ppm, respectively. Moreover, all the aromatic protons appear in their expected chemical shift. One of the characteristic features of ^{13}C NMR spectra of compounds **4a-e** is the disappearance of ketonic carbonyl due to its conversation to ketoxime group (C=N-OH) which appear at δ 152.8-153.65 ppm. Also, the methyl group attached to ketoxime appears at δ 11.64-12.07 ppm.

2.2. Biology

2.2.1. *In vitro* one dose full NCI 60 cell panel assay

Compounds **3a**, **3b**, **3e** and **4b** have been selected for *in vitro* anticancer screening by the National Cancer Institute. The results **(Table 1)** recorded that compound **3e** exhibited a remarkable anticancer activity against most of the tested cell lines. A complete cell death was observed against leukemia CCRF-CEM, HL-60(TB) cell lines, non-small cell lung cancer NCI-H522 cell line, colon cancer COLO205 cell line, CNS cancer SF-539 cell line, melanoma MDA-MB-435 cell line and breast cancer MDA-MB-468 cell line with growth percentages of -11.91%, -54.34%, -14.53%, -16.22%, -22.86%, -46.05% and -12.81%, respectively. A significant anticancer activity has been observed against the tested cell lines of leukemia, non-small cell lung cancer, colon cancer, melanoma cancer, ovarian cancer, renal cancer, prostate cancer and breast cancer cell lines with growth inhibition percentages of 58.41% up to 99.55% (**Table 1**). A moderate cell growth inhibition was observed against the rest of cell lines with growth inhibition percentages of 24.30% up to 48.11%. Finally, compounds **3a**, **3b** and **4b** showed a moderate cell growth inhibition against most of the tested cell lines with growth inhibition percentages of 20.06% to 56.20%, 20.54% to 32.06% and 20.51% to 41.90%, respectively (**Table 1**).

Table 1: Single concentration mean graph growth inhibition of nine different cancer cell types for compounds **3a**, **3b**, **3e** and **4b**

Subpanel cancer cell Lines	% Growth Inhibition (GI %)[a]			
	3a	**3b**	**3e**	**4b**
Leukemia				
CCRF-CEM	15.89	-9.5	**111.9**	**-13.0**
HL-60(TB)	51.46	**11.8**	154.3	-6.55
K-562	28.47	1.10	99.46	21.08
MOLT-4	28.72	-3.30	**96.16**	**-5.33**
RPMI-8226	13.93	-14.4	92.53	-12.6
SR	11.31	2.49	**92.38**	9.38
Non-small cell lung cancer				
A549/ATCC	14.01	14.67	80.22	22.97
EKVX	-0.77	-2.14	66.24	-2.49
HOP-62	19.26	-0.94	79.28	14.89
HOP-92	56.20	1.68	89.66	9.50
NCI-H226	5.64	9.04	41.54	13.18
NCI-H23	-2.77	2.83	61.61	8.86
NCI-H322M	-15.6	-0.95	54.71	-7.94
NCI-H460	-10.8	-11.4	94.21	-8.72
NCI-H522	21.22	32.06	114.5	32.95
Colon cancer				
COLO 205	6.12	-14.8	116.2	-14.7
HCC-2998	-14.5	-5.35	78.98	-0.39
HCT-116	37.64	23.71	96.08	20.51
HCT-15	2.31	-3.11	59.78	-9.07
HT29	-4.15	-1.38	93.18	11.69
KM12	-4.62	-1.48	83.25	0.23
SW-620	3.50	-11.9	74.17	-6.13
CNS cancer				
SF-268	-6.20	-0.59	73.15	7.31
SF-295	11.02	4.93	96.6	-1.33
SF-539	5.12	2.36	122.9	9.14
SNB-19	7.65	3.48	41.78	8.92
SNB-75	-12.1	11.73	61.87	9.52
U251	10.88	10.63	83.98	15.65
Melanoma				
LOX IMVI	2.96	3.84	81.51	17.24
MALME-3M	2.84	-2.75	30.49	-1.95

M14	16.40	12.41	94.83	20.6
MDA-MB-435	-0.55	-11.2	146.0	-5.70
SK-MEL-2	-3.79	-3.68	64.11	6.38
SK-MEL-28	1.20	-0.54	42.23	-3.87
SK-MEL-5	3.36	-0.45	84.75	2.13
UACC-257	5.25	15.34	46.34	20.27
UACC-62	4.32	-	64.04	-
Ovarian cancer				
IGROV1	-8.53	-5.76	61.55	-10.0
OVCAR-3	-6.48	-8.04	99.62	-4.14
OVCAR-4	-3.52	-7.54	38.52	2.46
OVCAR-5	-2.74	-2.73	48.11	-8.26
OVCAR-8	6.35	8.97	76.81	14.95
NCI/ADR-RES	-6.05	-8.37	24.3	2.61
SK-OV-3	15.88	20.54	65.44	39.51
Renal cancer				
786-0	11.75	5.27	64.53	-0.11
A498	18.04	1.90	81.52	-7.72
ACHN	-0.61	-0.51	58.41	4.19
CAKI-1	-0.45	3.76	38.45	12.89
RXF 393	-8.64	-7.57	75.44	-3.30
SN12C	-0.11	5.50	70.53	7.12
TK-10	-	1.64	-	12.08
UO-31	7.90	-5.03	50.65	9.64
Prostate cancer				
PC-3	39.38	11.97	81.96	0.88
DU-145	-8.73	-6.43	85.87	-1.04
Breast cancer				
MCF7	20.93	2.55	81.79	8.36
MDA-MB-231/ATCC	-6.88	4.80	80.27	19.80
HS 578T	0.42	-14.8	89.44	3.63
BT-549	20.06	17.77	63.15	14.05
T-47D	22.99	10.55	64.13	41.9
MDA-MB-468	0.83	-5.25	112.8	9.92

2.2.2 *In vitro* five dose full NCI 60 cell panel assay

In this context, compound **3e** recorded high activity against most of the cell lines tested with GI_{50} ranging from 19 to 100 μM (**Table 2**, **Fig. 4**) and selectivity ratios ranging between 0.75 and 1.71 at the GI_{50} level. Compound **3e** was found to be a broad-spectrum antitumor agent against different tumor subpanels tested without selectivity to the cell lines tested.

Table 2: *In vitro* five dose full NCI 60 cell panel assay of **3e**

Panel	Cell line	GI_{50}			TGI	LC_{50}
		Conc. per cell line	Subpanel MID^b	Selectivity ratio (MID^a/MID^b)	Conc. per cell line	
Leukemia	CCRF-CEM	31.60	31.60	1.71	>100	>100
	HL-60(TB)	35.00			>100	>100
	K-562	37.70			>100	>100
	MOLT-4	36.40			>100	>100
	RPMI-8226	29.90			>100	>100
	SR	19.00			>100	>100
Non-small cell lung cancer	A549/ATCC	>100	70.14	0.77	>100	>100
	EKVX	>100			>100	>100
	HOP-62	79.3			>100	>100
	HOP-92	22.60			>100	>100
	NCI-H226	89.80			>100	>100
	NCI-H23	>100			>100	>100
	NCI-H322M	30.30			>100	>100
	NCI-H460	39.10			>100	>100
	COLO 205	>100			>100	>100

Colon cancer	HCC-2998	>100	72.58	0.75	>100	>100
	HCT-116	42.10			>100	>100
	HCT-15	>100			>100	>100
	HT29	55.70			>100	>100
	KM12	63.60			>100	>100
	SW-620	46.70			>100	>100
CNS cancer	SF-268	68.70	48.23	1.12	>100	>100
	SF-295	43.00			>100	>100
	SF-539	29.60			>100	>100
	SNB-19	64.00			>100	>100
	SNB-75	28.50			>100	>100
	U251	55.60			>100	>100
Melanoma	LOX IMVI	41.70	44.54	1.22	>100	>100
	MALME-3M	48.10			>100	>100
	M14	37.40			>100	>100
	MDA-MB-435	24.30			87.60	>100
	SK-MEL-28	47.50			>100	>100
	SK-MEL-5	31.90			>100	>100
	UACC-257	97.40			>100	>100
	UACC-62	28.00			>100	>100
Ovarian cancer	IGROV1	53.40	66.81	0.81	>100	>100
	OVCAR-3	34.00			>100	>100
	OVCAR-4	82.90			>100	>100
	OVCAR-5	85.10			>100	>100
	OVCAR-8	73.70			>100	>100
	NCI/ADR-	>100			>100	>100

	RES					
	SK-OV-3	38.60			>100	>100
Renal cancer	786-0	41.70	55.97	0.968	>100	>100
	A498	21.30			85.00	>100
	ACHN	85.00			>100	>100
	RXF-393	40.10			>100	>100
	SN12C	70.20			>100	>100
	TK-10	96.90			>100	>100
	UO-31	36.60			>100	>100
Prostate cancer	PC-3	36.40	49.5	1.09	>100	>100
	DU-145	62.60			>100	>100
Breast cancer	MCF7	40.00	33.94	1.60	>100	>100
	MDA-MB-231/ATCC	38.70			>100	>100
	BT-549	32.00			99.70	>100
	T-47D	34.00			>100	>100
	MDA-MB-468	25.40			>100	>100
MID[a]			54.16			

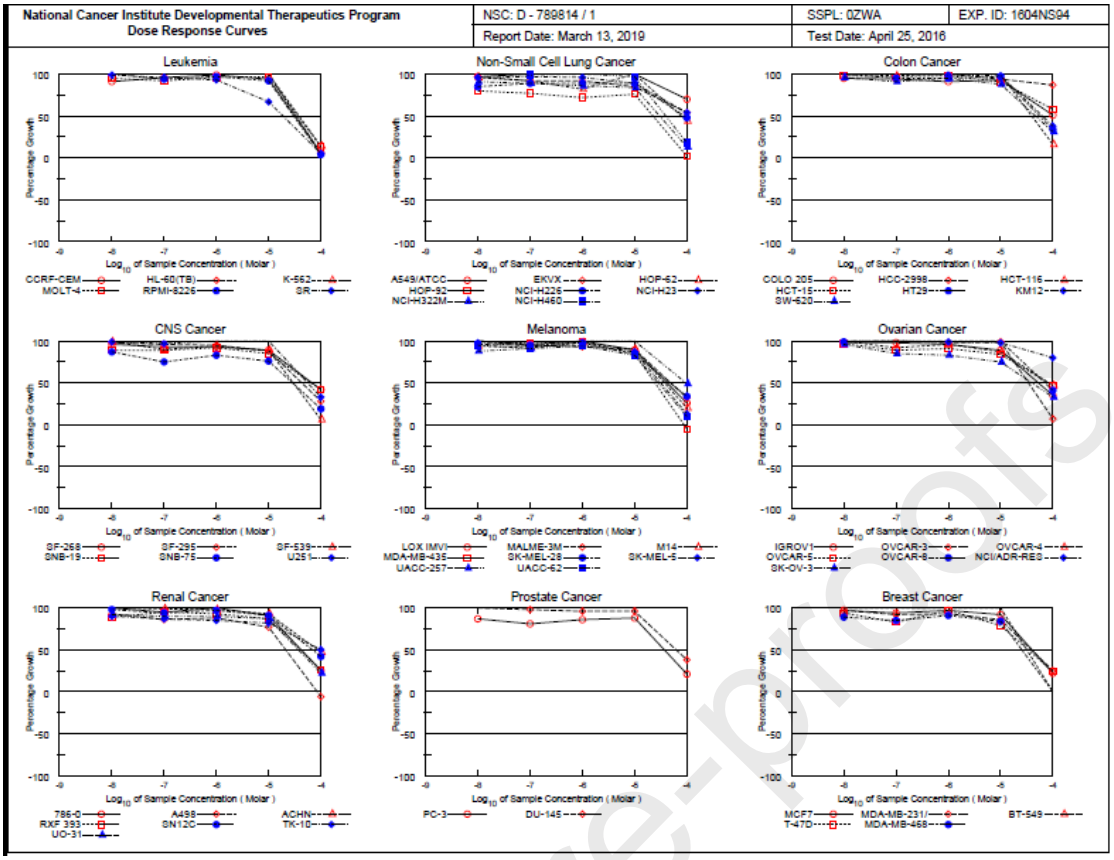

Fig. 4. Dose-antiproliferative response of compound **3e** against nine different cancer cell lines

2.2.3. VEGFR-2 Assay

The overexpression of several kinases in endothelial cells indicated its crucial role in angiogenesis and vasculogenesis of cancers [24]. Of these protein kinases, VEGFR-2 plays an important role in the survival/proliferation of endothelial cells and the development of cancers [25, 26]. VEGFR-2-kinase was assayed with kinase-glo-luminescent kinase assays against **3a**, **3b**, **3e**, **4b** and **Sorafenib** as a reference (**Table 3**).

Table 3: The enzymatic inhibitory activities against VEGFR-2 for compounds **3a**, **3b**, **3e** and **4b**.

Compound	IC_{50} (nμ)
3a	386.4
3b	> 1000
3e	198.7
4b	> 1000
Sorafenib	0.17

Of these, **3a** and **3e** were the most potent analogues with IC_{50} values of 386.4 nM and 198.7 nM against VEGFR-2, respectively, in comparison to Sorafenib (IC_{50}= 0.17 nM). The results show that introduction of 3,4,5-trimethoxy substituent on the phenyl ring was favorable the activities while introduction of 4-methoxy substituent or oxime moiety decrease the activity.

2.2.4. Cell cycle analysis and apoptosis detection

2.2.4.1. Cell cycle analysis

Studies were carried out on the effect of the **3e** compound on leukemia cell cycle growth and apoptosis. Leukemia SR cells have been incubated at an IC_{50} level of **3e** for 24 h. The study results (**Fig. 5**) show that the compound **3e** apoptosis levels of Leukemia SR pre-G1 was 17.34%. In Leukemia SR treated with **3e**, a high percent of cell accumulation was observed in the G2 / M phase (34.36%) indicating cell cyclic arrest at G2 / M transformation.

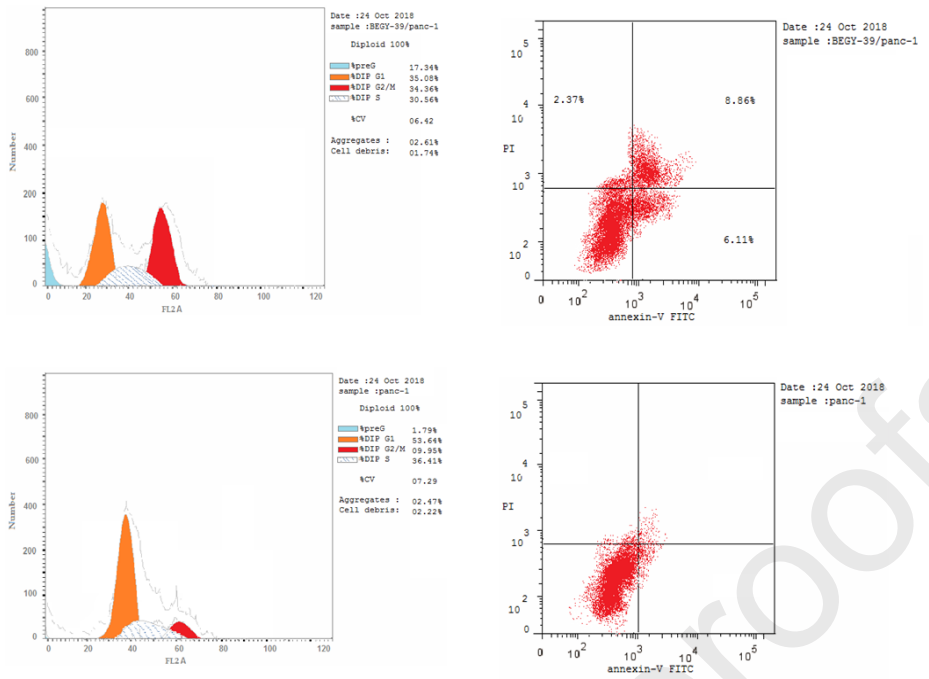

Fig. 5. Cell cycle analysis in Leukemia SR cell line treated with compound **3e**

2.2.4.2. Apoptosis assay

Leukemia SR cell cycle research has shown that the signalling of preG1 apoptosis occurs after **3e** action. cells were incubated with annex V/PI for 24 h to check **3e** for apoptosis. Early and late apoptosis studies show that 3e is likely to cause significant apoptosis with 2.37% necrosis, **(Table. 4)**.

Table 4. Apoptosis detection of **3e** in Leukemia SR cancer cell line

Compound	**Apoptosis**			**Necrosis**
	Total	**Early**	**Late**	
3e / Leukemia SR	17.34	6.11	8.86	2.37
Cont. Leukemia SR	1.79	1.02	0.47	0.3

2.3. Docking study into VEGFR-2

In the present study, compounds **3a** and **3e** exhibited inhibitory activity against VEGFR-2 protien kinase with IC_{50} values in the nanomolar range, **Table 3**. Accordingly, a comparative molecular docking study of the new compounds into the ATP active site of VEGFR-2 (PDB code: 4ASD) was performed. The crystal struture of the VEGFR-2 tyrosine kinase [22] co-crystallized with sorafenib was obtained from the protein data bank (https://www.rcsb.org/structure/4asd). The docking study was performed using AutoDock 4.2. [32]. Ligands and protein files were prepared using AutoDock tools according to the previous reports [33,34]. Grid and docking parameter files were prepared according to the previous reports [35,36]. The 2/3D binding modes of the new compounds sorafenib were generated using discovery studio visualizer [25] and LigPlot^{+} (v.2.1) [26].

Validation of the docking procedures was performed by re-coking sorafenib into the active site of VEGFR-2. The results revealed the superposition of the sorafenib over the co-crystallized ligand with RMDS of 1.01 Å. In addition, the re-docked sorafenib showed the same binding interactions with VEGFR-2 like the co-crystallized ligand, **Fig. 6**. The re-docked sorafenib exhibited three conventional hydrogen bonds with Glu885, Cys919, and Asp1046 amino acids. In addition, several hydrophobic interactions with Val848, Ala866, Leu889, Val916, Leu1035, Cys1045, and Phe1047 amino acids were also observed.

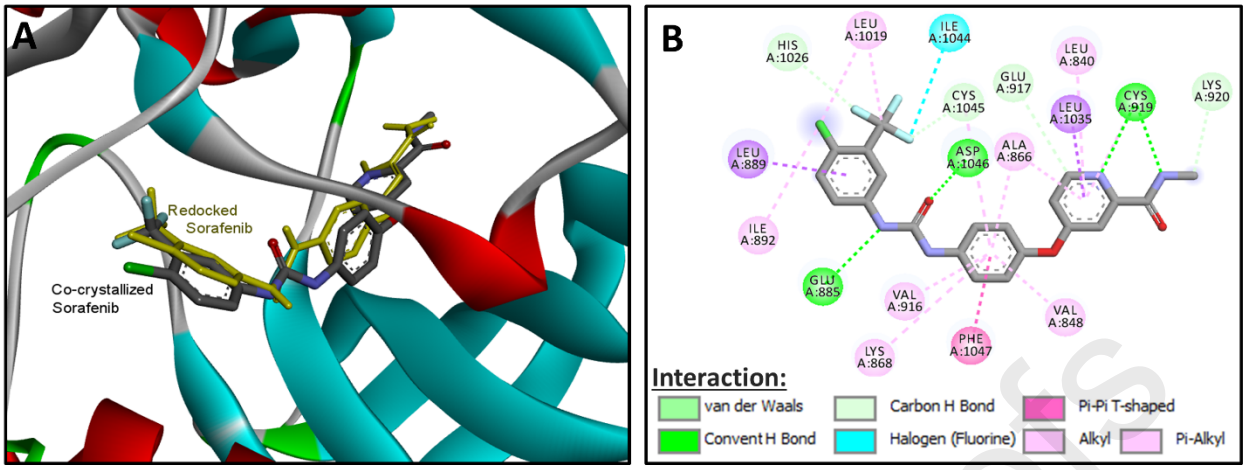

Fig. 6: Binding mode/interactions of redocked/co-crystallized sorafenib into the active of VEFGR-2 (PDB code: 4ASD): A) 3D binding modes showing superimposition of the re-docked ligand (Sorafenib, shown as sticks, colored in yellow) over the native cocrystallized ligand (sorafenib, shown as sticks, colored by element) into the active site of VEGFR-2, RMSD = 1.01 Å; B) 2D binding mode of the re-docked sorafenib into VEGFR-2 showing H-bonding and hydrophobic interactions, hydrogen atoms were omitted for clarity.

The results of the docking study also revealed nice fitting of the new compounds (**3a-e** and **4-e**) into the active site of VEGFR-2, **Fig. 7**. The new compounds showed binding free energies (ΔG_b) in the range of -9.80 to -11.25 kcal/mol and inhibition constant (K_i) in the range of 5.69-66.05 nM, compared to a binding free energy of -12.12 kcal/mol and inhibition constant of 1.31 nM for sorafenib. Generally, the compounds **4a-e** exhibited higher affinities toward VEGFR-2 than their parent derivatives **3a-e**. This could be attributed to the presence of hydroxyimino moiety in compound **4a-e** which formed a cluster of hydrogen bonds with amino acids in VEGFR-2. The best fit conformation of most of the new compounds exhibited binding orientations similar to sorafenib and displayed similar binding interactions with the key amino acids in the active site of VEGFR-2. The 4-(un)substituted-phenyl-1,6-dihydropyrimidine moiety of the new compounds displayed multiple hydrophobic interactions similar to the 4-chloro-3-(trifluoromethyl)phenyl moiety in sorafenib. Moreover, the acetyl/ hydroxyimino moities of the new compounds formed

different hydrogen-bonding interactions like the *N*-methylcarboxamide moiety in sorafenib, **Fig. 3**. However, **3b** and **4b** exhibited different binding orientations from sorafenib which can account of their weak inhibitory activity against VEGFR-2, **Table 3**.

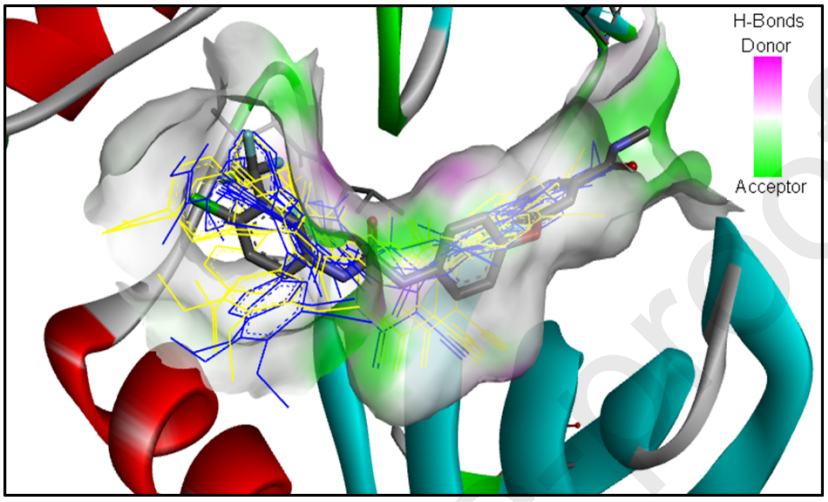

Fig. 7. 3D binding modes of compounds **3a-e** (shown as yellow lines) and compounds **4a-e** (shown as blue lines) overlaid with the native co-recrystallized sorafenib (shown as sticks colored by element) into the active site of VEGFR-2, receptor shown as H-bond surface, hydrogen atoms were hidden for clarity

The results of the docking study of compounds **3a-e** revealed binding free energy in the range of -9.80 to -10.86 kcal/mol compared to -12.12 kcal/mol for sorafenib. Among these derivatives, compound **3e** exhibited a binding free energy of -10.19 kcal/mol. These results were quite matched with the IC_{50} values of sorafenib and compounds **3**, **Table 3**. Investigation of the binding mode of compound **3e** revealed similar binding orientation/interactions to those of the co-crystallized sorafenib. Three conventional hydrogen bonds were observed between compound **3e** and Lys868, Glu885, and Asp1046 with bond length in the range of 1.59-2.61Å. Moreover, compound **3e** formed three carbon-hydrogen bonds with Leu840, Phe918, and CYS919 amino acids with bond length in the range of 1.97-2.30 Å. Like sorafenib, compound **3e** also displayed several hydrophobic interactions with, Val848, Ala866,

Val899, Val916, His1026, Leu1035, and Cys1045 amino acids in VEGFR-2, **Fig. 8**. The high similarity between hydrogen bonding/hydrophobic interactions of compound **3e** and sorafenib could account for its high inhibitory activity against VEGFR-2, **Table 3**.

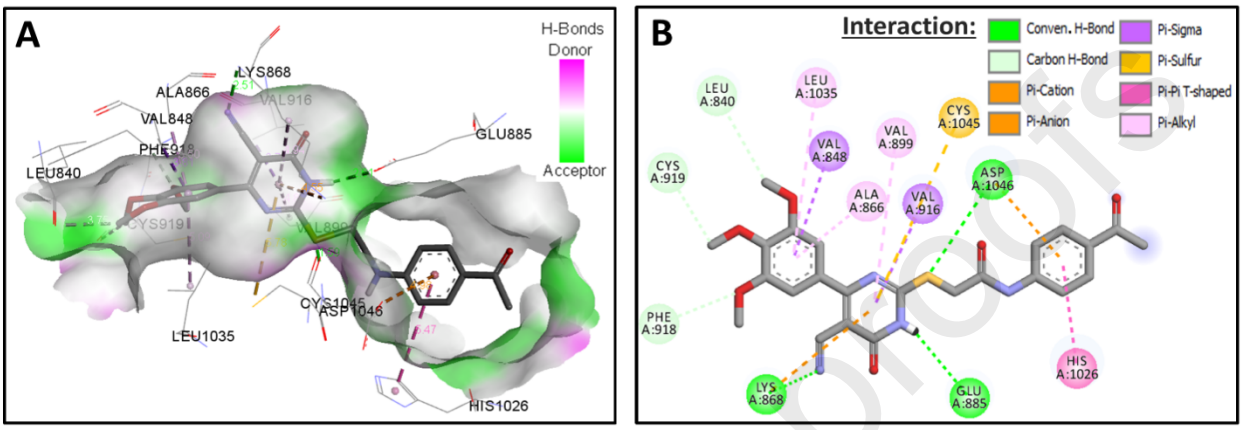

Fig. 8. Binding modes/interactions of compound **3e** into VEGFR (PDB code: 4ASD): A) 3D binding mode of compound **3e** (shown as stick, colored by element), receptor surface shown as H-bond donor (pink) and acceptor (light green); B) 2D binding mode of compound **3e (**shown as stick, colored by element); hydrogen atoms were omitted for clarity.

In addition, compound **3a** exhibited three conventional hydrogen bonds with Glu885, Cys919, and Asp1046 amino acids in VEGFR, **Fig. 9**. These hydrogen bonds were identical with the three hydrogen bonds formed by sorafenib, **Fig. 6**. In addition, compound **3a** showed several types of hydrophobic interactions with Val848, Ala866, Leu889, Leu1019, Leu1035, Ile1044, and Cys1045 amino acids, like those observed with sorafenib.

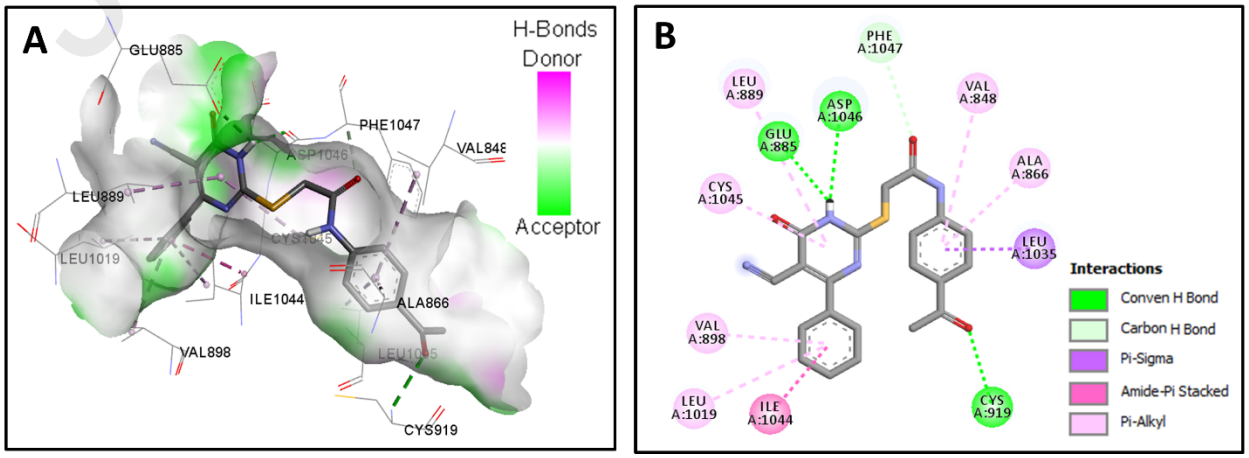

Fig. 9. Binding modes/interactions of compound **3a** into VEGFR(PDB code: 4ASD): A) 3D binding mode of compound 3a (shown as stick, colored by element), receptor surface shown as H-bond donor (pink) and acceptor (light green); B) 2D binding mode of compound **3a (**shown as stick, colored by element); hydrogen atoms were omitted for clarity.

On the other hand, the results of the docking study of compounds **3b** and **4b** revealed binding free energies of-10.86 and -10.69 kcal/mol. However, compounds **3b** and **4b** exhibited weaker inhibitory activities toward VEGFR-2 compared to compounds **3a**,**e**, **Table 3**. Molecular docking analyses of the best-fit conformations of compounds **3b** and **4b** revealed completely different binding orientations from those of sorafenib and compounds **3a**,**e**, **Fig. 10**. This difference in the orientation could account for their weak inhibitory activity against VEGFR-2.

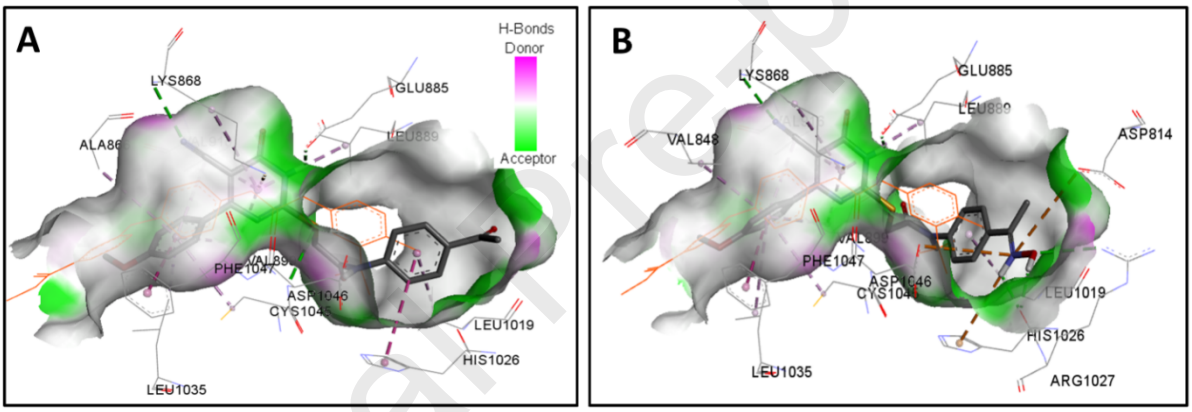

Fig. 10. 3D Binding modes of compound **3b** and **4b** into VEGFR(PDB code: 4ASD): A) 3D binding mode of compound **3b** (shown as stick, colored by element), overlaid with sorafenib (shown as orange line); B) 3D binding mode of compound **4b** (shown as stick, colored by element), overlaid with sorafenib (shown as orange line), receptor shown as H-bond surface.

Furthermore, LigPlot views of the best fit conformation of compounds **3b** and **4b** were generated showing different types of interactions with VEGFR-2, **Fig. 11**. Compounds **3b** and **4b** displayed two and five hydrogen bonds with VEGFR-2, respectively. The fewer number of hydrogen bonds observed for compound **3b** could also account for its weak inhibitory activity against VEGFR-2, **Table 3**. In addition, compound **4b** displayed one hydrogen bond with Glu885, while the remaining four hydrogen bonds

were formed with Ile1025, His1026, and Arg1027 indicating different interaction pattern from sorafenib and compounds **3a**,**e**. The difference in the binding interactions of compound **4b** could also account for its weak inhibitory activity toward VEGFR-2.

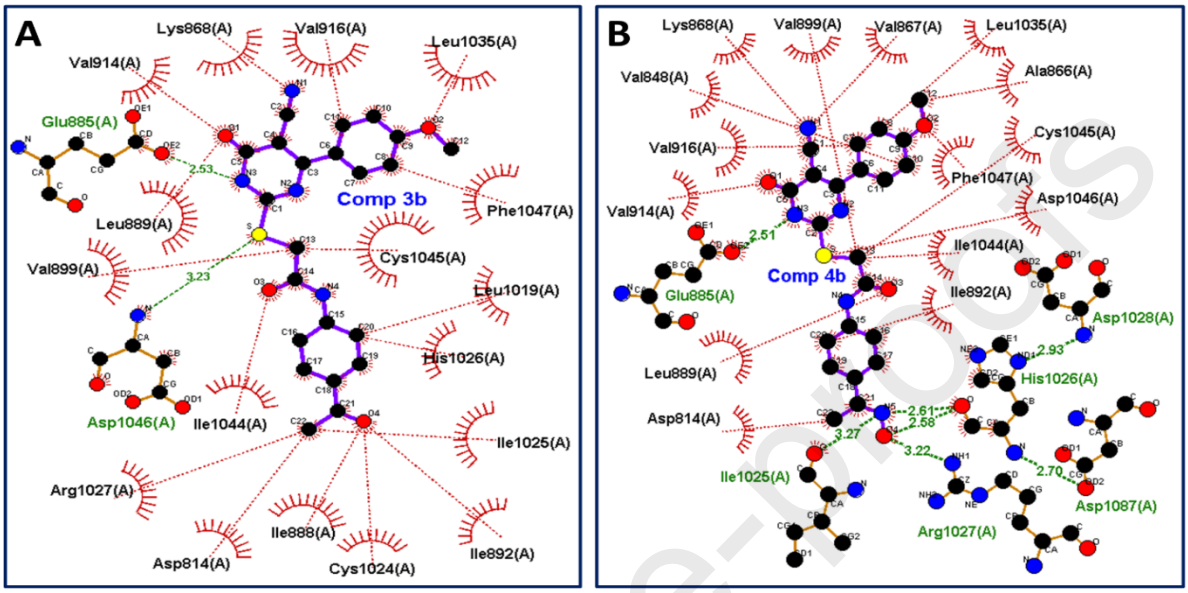

Fig. 11: LigPlot view of compound **3b** and**4b**:A) LigPlot view of compound **3b** into the binding site ofVEGFR-2 (PDB code: 4ASD) showing two conventional hydrogen bonds with Glu885 and Asp1046; B) LigPlot view of compound **4b**into VEGFR-2 showing five hydrogen bonds with Glu885, Ile1025, His1026 and Arg1027; hydrophobic interactions shown as brick red dotted lines and hydrogen bonding interactions shown as olive green dotted lines.

3- CONCLUSION

A series of novel 1,6-dihydropyrimidine-2-thio derivatives targeting VEGFR-2 were developed and synthesized. Compounds **3a**, **3b**, **3e** and **4b** have been selected for *in vitro* anticancer screening by the National Cancer Institute. The results recorded that compound **3e** exhibited a remarkable anticancer activity against most of the tested cell lines. where a complete cell death was observed against. *In vitro* five dose full NCI 60 cell panel assay results revealed that **3e** showed high activity against most of the cell lines tested with GI_{50} ranging from 19 to 100 μM and selectivity ratios ranging between 0.75 and 1.71 at the GI_{50} level. Compound **3e** was found to be a broad-spectrum antitumor agent against different tumor subpanels tested without selectivity to the cell lines tested. A molecular docking study was performed to evaluate binding modes, affinities and interactions of the new compounds into the active site of VEGFR-2. The results of the docking study revealed nice fitting of the new compounds into the active site of VEGFR-2 with binding free energies in the range of -9.80 to -11.25 kcal/mol compared to -12.12 kcal/mol for sorafenib. Compounds **4a-e** with the hydroxyimino group exhibited higher binding affinities toward VEGFR-2 than their parent derivatives **3a-e**. Compound **3a** and **3e** which showed similar binding modes and interactions to sorafenib. On the other hand, compounds **3b** and **4b** exhibited completely different orientations from sorafenib which resulted in different interaction patterns into VEGFR-2.

4. EXPERIMENTAL

4.1. Chemistry

General details **[See appendix A]**

Compounds **1a-e** and **2** [28] were prepared according to previous reported procedures.

4.1.1. General procedure for synthesis of *N*-(4-acetylphenyl)-2-(5-cyano-4-oxo-6-(substituted phenyl)-1,6-dihydropyrimidin-2-ylthio) acetamide (3a-e)

A mixture of appropriate pyrimidine derivative **1a-e** (1 mmol), compound **2** (1 mmol) and anhydrous K_2CO_3 (0.167 g, 1.2 mmol) in 50 mL acetone was heated at reflux for 4-8 hours, then 20 mL of distilled water was added, the precipitate was filtered off, washed with distilled water, dried and crystallized from absolute ethanol affording the target products **3a-e**

4.1.1.1. *N*-(4-Acetylphenyl)-2-(5-cyano-4-oxo-6-phenyl-1,6-dihydro-pyrimidin-2-ylthio)acetamide (3a)

Yellowish white powder in (0.38 g, 95% yield); mp: 200-202 ˚C; IR (KBr), ν_{max}/cm^{-1}; 3453 (N-H), 2212 (CN), 1674 (CO-NH), 1592 (C=N); ^{1}H NMR (DMSO-d_6) δ (ppm): 2.49 (s, 3H, CH_3), 3.87 (s, 2H, CH_2), 7.36-7.46 (m, 3H, Ar-H+NH), 7.67 (d, 2H, J = 8.0 Hz, Ar-H), 7.74 (d, 2H, J = 8.00 Hz, Ar-H), 7.89 (d, 2H, J = 8.00 Hz, Ar-H), 11.17 (s, 1H, NH); ^{13}C NMR (DMSO-d_6) δ (ppm): 26.75, 35.64, 89.83, 118.48, 120.04, 128.45, 128.49, 129.87, 130.25, 131.92, 137.63, 143.73, 167.60, 168.66, 170.52, 171.82, 196.92. HRMS (ESI) calcd. for $C_{21}H_{15}N_4O_3S$ [M-H]: 403.0870, found: 403.0872.

4.1.2.2. *N*-(4-Acetylphenyl)-2-(5-cyano-6-(4-methoxyphenyl)-4-oxo-1,6-dihydropyrimidin-2-ylthio)acetamide (3b)

Yellow powder in (0.37 g, 86% yield); mp: 195-197 ˚C; IR (KBr), ν_{max}/cm^{-1}: 3321 (N-H), 2204 (CN), 1699 (CO-CH_3), 1674 (CO-NH), 1653 (C=N), 1606 (C=C), 1313 (C-O). ^{1}H NMR (DMSO-d_6) δ (ppm): 2.4 (s, 3H, CH_3), 3.75 (s, 3H, OCH_3), 3.84 (s, 2H, CH_2), 6.92 (d, 2H, J = 8.00 Hz, Ar-H), 7.68 (d, 2H, J = 8.00 Hz, Ar-H), 7.74 (d, 2H, J = 8.0 Hz, Ar-H), 7.90 (2H, d, J = 8.0 Hz, Ar-H), 11.28 (s, 1H, NH); ^{13}C NMR (DMSO-d_6) δ (ppm): 26.49, 35.35, 55.30, 88.70, 113.48, 118.14, 120.14, 129.61, 129.85, 131.62, 143.20, 143.51, 160.67, 166.54, 168.44, 170.23, 171.30, 196.50. HRMS (ESI) calcd for $C_{22}H_{17}N_4O_4S$ [M-H]: 433.0976, found: 433.0979.

4.1.1.3. *N*-(4-Acetylphenyl)-2-(5-cyano-6-(3-methoxyphenyl)-4-oxo-1,6-dihydropyrimidin-2-ylthio)acetamide (3c)

Yellowish white powder in (0.36 g, 84% yield); mp: 205-207 ˚C; IR (KBr), ν_{max}/cm^{-1}: 3329 (N-H), 2212 (CN), 1674 (CO-NH), 1595 (C=N), 1303 (C-O); ^{1}H NMR (DMSO-d_6) δ (ppm): 2.50 (s, 3H, CH_3), 3.74 (s, 3H, OCH_3), 3.87 (s, 2H, CH_2), 7.02 (d, 1H, J = 8.00 Ar-H), 7.30-7.33 (m, 3H, Ar-H), 7.67 (d, 2H, J = 8.0 Hz, Ar-H), 7.89 (d, 2H, J = 8.0 Hz, Ar-H), 11.18 (s, 1H, NH), ^{13}C NMR (DMSO-d_6) δ (ppm): 26.54, 35.39, 55.24, 89.70, 113.61, 115.66, 118.27, 119.77, 120.60, 129.39, 129.64, 131.71, 138.74, 143.49, 158.97, 167.18, 168.41, 170.20, 171.53, 196.70. HRMS (ESI) calcd for $C_{22}H_{17}N_4O_4S$ [M-H]: 433.0976, found: 433.0979.

4.1.1.4. *N*-(4-Acetylphenyl)-2-(5-cyano-6-(3,4-dimethoxyphenyl)-4-oxo-1,6-dihydropyrimidin-2-ylthio)acetamide (3d)

Yellowish brown powder in (0.24 g, 51% yield); mp: 180-181 ˚C; IR(KBr), ν_{max}/cm^{-1}: 3321 (N-H), 2200 (CN), 1675 (C=O), 1653 (CO-NH), 1646 (C=N), 1606 (C=C),

1313 (O-CH_3); ^{1}H NMR (DMSO-d_6) δ (ppm): 2.5 (s, 3H, CH_3), 3.74 (s, 3H, OCH_3), 3.77 (s, 3H, OCH_3), 3.85 (s, 2H, CH_2), 6.96 (d, 1H, J = 8.00 Hz, Ar-H), 7.40-7.41 (m, 2H, Ar-H), 7.67 (d, 2H, J = 8.00 Hz, Ar-H), 7.90 (2H, d, J = 8.00 Hz, Ar-H), 11.29 (1H, s, NH); ^{13}C NMR (DMSO-d_6) δ (ppm): 26.28, 34.99, 55.29, 55.39, 88.67, 110.80, 111.46, 117.96, 120.00, 121.69, 129.41, 131.44, 143.28, 147.88, 150.14, 165.82, 166.46, 168.25, 170.40, 171.00, 196.38. HRMS (ESI) calcd for $C_{23}H_{19}N_4O_5S$ [M-H]: 463.1082, found: 463.1089.

4.1.1.5. ***N*-(4-Acetylphenyl)-2-(5-cyano-4-oxo-6-(3,4,5-trimethoxyphenyl)-1,6-dihydropyrimidin-2-ylthio)acetamide (3e)**

Yellowish brown powder in (0.30 g, 60% yield); mp: 178-180 ˚C; IR (KBr), ν_{max}/cm^{-1}: 3307 (N-H), 2193 (CN), 1677 (CO-NH), 1620 (C=N), 1598 (C=C), 1327 (C-O); ^{1}H NMR (DMSO-d_6) δ (ppm): 2.5 (s, 3H, CH_3), 3.69 (s, 3H, OCH_3), 3.76 (s, 6H, 2OCH_3), 3.85 (s, 2H, s, CH_2), 7.11 (s, 2H, Ar-H), 7.65 (d, 2H, J = 8.80 Hz, Ar-H), 7.88 (2H, d, J = 8.80 Hz, Ar-H), 11.26 (s, 1H, NH); ^{13}C NMR (DMSO-d_6) δ: 26.51, 35.32, 55.97, 60.18, 89.41, 103.82, 105.84, 111.80, 118.21, 120.03, 129.62, 131.68, 132.60, 138.94, 143.45, 152.47, 166.93, 168.40, 170.10, 171.28, 196.29. HRMS (ESI) calcd for $C_{24}H_{21}N_4O_6S$ [M-H]: 493.1187, found: 493.1193.

4.1.2. General procedure for synthesis of 2-(5-cyano-6-oxo-4-(substituted)-phenyl-1,6-dihydropyrimidin-2-ylthio)-*N*-(4-(1-(hydroxylimino)-ethyl)phenyl) acetamide (4a-e)

A mixture of the appropriate ketone derivatives **3a-e** (0.3 mmol) and hydroxylamine hydrochloride (0.021 g, 0.3 mmol) in 30 mL of absolute ethanol was heated under reflux for 8-12 hours and then left to cool to room temperature. The separated solid

was filtered off, washed with 10% ammonia solution and then with distilled water, dried, and recrystallized from absolute ethanol affording the target products **4a-e**

4.1.2.1. 2-(5-Cyano-6-oxo-4-phenyl-1,6-dihydropyrimidin-2-ylthio)-*N*-(4-(1-(hydroxyimino)ethyl)phenyl)acetamide (4a)

Yellowish white powder in (0.09 g, 70% yield); mp: 198-200 ˚C; IR (KBr), ν_{max}/cm^{-1}: 3321 (OH), 2342 (CN), 1687 (CONH), 1671 (C=NH), 1596 (C=C). ^{1}H NMR (DMSO-d_6) δ (ppm): 2.14 (s, 3H, CH_3), 4.21 (s, 2H, CH_2), 7.32-7.53 (4H, m, Ar-H + NH), 7.59 (d, 2H, J = 8.0 HZ, Ar-H), 7.64 (d, 2H, J = 8.0 HZ, Ar-H), 7.86 (2H, d, J = 8.0 Hz, Ar-H), 10.45 (s, 1H, OH), 11.10 (s, 1H, NH); ^{13}C NMR (DMSO-d_6) δ (ppm): 11.92, 39.98, 93.41, 116.38, 119.30, 126.61, 128.88, 129.21, 132.30, 132.49, 135.37, 139.57, 153.30, 161.75, 165.97, 166.31, 167.77. HRMS (ESI) calcd for $C_{21}H_{16}N_4O_3S$ [M-H]: 418.0979, found: 418.0983.

4.1.2.2. 2-(5-Cyano-4-(4-methoxyphenyl)-6-oxo-1,6-dihydropyrimidin-2-yl-thio)-*N*-(4-(1-(hydroxyimino)ethyl)phenyl)acetamide (4b)

White powder in (0.098 g, 65% yield); mp: 240-243 ˚C; IR (KBr), ν_{max}/cm^{-1}: 3000-3500 (br, NH, OH), 2223 (CN), 1650 (CO-NH), 1619 (C=N), 1595 (C=C), 1332 (C-O). ^{1}H NMR (DMSO-d_6) δ (ppm): 2.13 (s, 3H, CH_3), 3.79 (s, 3H, OCH_3), 3.93 (s, 2H, CH_2), 6.92 (d, 2H, J = 8.0 Hz, Ar-H), 7.15-7.55 (m, 4H, Ar-H), 7.83 (d, 2H, J = 8.0 Hz, Ar-H), 10.86 (s, 1H, OH), 11.08 (s, 1H, NH). ^{13}C NMR (DMSO-d_6) δ (ppm): 12.07, 35.98, 55.96, 91.04, 114.27, 117.91, 119.44, 126.75, 128.15, 131.22, 132.58, 139.76, 153.65, 162.34, 165.20, 166.96, 167.19, 167.62. HRMS (ESI) calcd for $C_{22}H_{18}N_5O_4S$ [M-H]: 448.1085, found: 448.1091.

4.1.2.3. 2-(5-Cyano-4-(3-methoxyphenyl)-6-oxo-1,6-dihydropyrimidin-2-yl-thio)-*N*-(4-(1-(hydroxyimino)ethyl)phenyl)acetamide (4c)

white powder in (0.09 g, 60% yield); mp: 170-175 ˚C; IR (KBr), ν_{max}/cm^{-1}: 3100-3588 (br, NH, OH), 2216 (CN), 1671 (CONH), 1598 (C=C), 1303 (C-O). ^{1}H NMR (DMSO-d_6) δ (ppm): 2.12 (s, 3H, CH_3), 3.76 (s, 3H, OCH_3), 3.92 (s, 2H, CH_2), 7.06 (d, 2H, J = 8.00 Hz, Ar-H), 7.32-7.57 (m, 4H, Ar-H), 7.59 (d, 2H, J = 8.00 HZ Ar-H), 10.86 (s, 1H, OH), 11.08 (s, 1H, NH). ^{13}C NMR (DMSO-d_6) δ (ppm): 11.91, 35.50, 55.62, 90.20, 108.50, 114.2, 115.60, 119.37, 121.31, 126.53, 130.09, 132.41, 136.50 139.49, 153.43, 159.38, 165.10, 166.10, 167.20, 167.30; HRMS (ESI) calcd for $C_{22}H_{18}N_5O_4S$ [M-H]: 448.1085, found: 448.1088.

4.1.2.4. 2-(5-Cyano-4-(3,4-dimethoxyphenyl)-6-oxo-1,6-dihydropyrimidin-2-ylthio)-*N*-(4-(1-(hydroxyimino)ethyl)phenyl)acetamide (4d)

White powder in (0.07 g, 52% yield); mp: 209-210 ˚C; IR (KBr), ν_{max}/cm^{-1}: 3322 (OH), 2200 (CN), 1687 (CO-NH), 1658 (C=N), 1596 (C=C), 1331 (C-O); ^{1}H NMR (DMSO-d_6) δ (ppm): 2.12 (3H, s, CH_3), 3.73 (s, 3H, OCH_3), 3.79 (s, 3H, OCH_3), 3.98 (s, 2H, CH_2), 6.93 (d, 1H, J = 8.00 Hz, Ar-H), 7.49 (d, 2H, J = 8.0 Hz, Ar-H), 7.56 (d, 2H, J = 8.0 Hz, Ar-H), 7.59 (d, 2H, J = 8.00 Hz, Ar-H), 10.80 (s, 1H, OH), 11.07 (s, 1H, NH). ^{13}C NMR (DMSO-d_6) δ (ppm): 11.90, 35.70, 55.91, 56.05, 90.05, 111.47, 112.08, 117.80, 118.80, 119.28, 122.69, 126.57, 128.68, 132.40, 139.66, 148.53, 151.55, 153.33, 167.18, 167.35, 168.50; HRMS (ESI) calcd for $C_{23}H_{20}N_5O_5S$ [M-H]: 478.1191, found: 478.1194.

4.1.2.5. **2-(5-Cyano-6-oxo-4-(3,4,5-trimethoxyphenyl)-1,6-dihydro-pyrimidin-2-ylthio)-*N*-(4-(1-(hydroxyimino)ethyl)phenyl)acetamide (4e)**

Yellow powder in (0.08 g, 54% yield); mp: 220 ˚C; IR (KBr), ν_{max}/cm^{-1}: 3100-3495 (br, NH, OH), 2213 (CN), 1664 (CONH), 1591 (C=C), 1326 (C=C). ^{1}H NMR (DMSO-d_6) δ (ppm): 2.12 (s, 3H, CH_3), 3.73 (s, 3H, OCH_3), 3.76 (s, 6H, $2OCH_3$), 4.26 (s, 2H, CH_2), 7.25 (s, 2H, Ar-H), 7.55 (d, 2H, J = 8.0 Hz, Ar-H), 7.59 (d, 2H, J = 8.0 Hz, Ar-H), 10.60 (s, 1H, OH), 11.08 (s, 1H, NH); ^{13}C NMR (DMSO-d_6) δ (ppm): 11.64, 35.50, 56.20, 60.48, 90.40, 106.81, 119.11, 126.30, 132.34, 134.20, 135.20, 141.10, 149.10, 149.80, 152.80,, 159.50, 166.70, 167.2, 167.3; HRMS (ESI) calcd for $C_{24}H_{22}N_5O_6S$ [M-H]: 508.1296, found: 508.1301

4.2. Biological activity

4.2.1 Evaluation of *in vitro* antiproliferative activity for compounds selected by NCI

The methodology of the NCI anticancer screening has been described in detail elsewhere (http://www.dtp.nci.nih.gov) [37]. **See Appendix A**

4.2.2. VEGFR-2 inhibitory assay

The inhibitory effect of **3a**, **3b**, **3e** and **4b** against VEGFR-2 was determined using enzyme-linked immunosorbent assays (ELISAs) [38]. **See Appendix A**

4.2.3. Cell apoptosis assay

Apoptosis was determined by flow cytometry based on the Annexin-V-fluoresce in isothiocyanate (FITC) and propidium iodide (PI) staining kit (BD Pharmingen, San Diego, USA) [39, 40]. **See Appendix A**.

4.3. Molecular docking study

The crystal structure of VEGFR-2 (PDB code: 4ASD) co-crystallized with sorafenib was downloaded from the protein data bank (https://www.rcsb.org/structure/4asd). The protein file of VEGFR-2 was prepared into the pdbqt format using AutoDock 4.2 [32]. The ligand files of the new compounds were sketched and converted to the PDB formats, their energies were minimized and prepared into the pdbqt format according to the previous reports [33, 34]. Grid and docking parameter files were prepared according to the previous reports [30, 31]. Discovery studio visualizer [25] and ligPlot LigPlot^{+} (v.2.1) [26] were used to visualize the binding modes, orientations, and interactions of sorafenib and the new compounds. The results of the docking study were presented in **Figures 6-11** and in supplementary data files (**Figures S5-10**).

Conflicts of interest

The authors declare no conflict of interest

5. References

1- C. Jin, Y.-J. Liang, H. He, L. Fu, Synthesis and antitumor activity of ureas containing pyrimidinyl group, Eur. J. Med. Chem. 46 (2011) 429-432.

2- P. Biginelli, P. Gazz. Synthesis of 3,4-Dihydropyrimidin-2(1H)-Ones, Chim. Ital. 23 (1893) 360-413.

3- A. T. Taher, S. M. Abou-Seri, Synthesis and bioactivity evaluation of new 6-aryl-5-cyano thiouracils as potential antimicrobial and anticancer agents. MOLEFW. 17 (2012) 9868-9886.

4- A. N. Chiang, J. C.Valderramos,R. Balachandran, R. J. Chovatiya, B. P. Mead, C.Schneider, S. L. Bell, M. G. Klein, D. M Huryn, X. S. Chen, Select pyrimidinones inhibit the propagation of the malarial parasite, Plasmodium falciparum. Bioorg. Med. Chem.17 (2009) 1527-1533.

5- T. C. Eadsforth, A.Pinto, R.Luciani, L. Tamborini, G. Cullia, C. De Micheli, L. Marinelli, S. Cosconati, E. Novellino, L. Lo Presti, Characterization of 2, 4-Diamino-6-oxo-1, 6-dihydropyrimidin-5-yl Ureido Based Inhibitors of Trypanosoma brucei FolD and Testing for Antiparasitic Activity. J. Med. Chem. 58 (2015) 7938-7948.

6- O. Fathalla, I. Zeid, M.Haiba, A. Soliman, S. I. Abd-Elmoez, W. El-Serwy, Synthesis, antibacterial and anticancer evaluation of some pyrimidine derivatives. World J. Chem. 4 (2009), 127-132.

7- J. C. Legeay, J. J. V. Eynde, J. P. Bazureau, A new approach to N-3 functionalized 3, 4-dihydropyrimidine-2 (1H)-ones with 1, 2, 4-oxadiazole group as amide isostere via ionic liquid-phase technology. Tetrahedron lett. 48 (2007), 1063-1068.

8- S. A.Abdel-Aziz, A. Nawal, H. Y. Hassan, A. F. Youssef, M. M. Yousri, synthesis of substituted dihydropyrimidines as hypotensive agents. B Pharm Sci. 34 (2011) 159-179.

9- E.Klein, S. DeBonis, B.Thiede, D. A. Skoufias, F. Kozielski,; L. Lebeau, New chemical tools for investigating human mitotic kinesin Eg5. Bioorg. Med. Chem. 15 (2007) 6474-6488.

10- M.M. Edrees, T.A. Farghaly, F.A.A. El-Hag, M.M. Abdalla, Antimicrobial, Antitumor, and 5α-reductase inhibitor activities of some hydrazonoyl substituted pyrimidinones. Eur. J. Med. Chem., 45 (2010) 5702-5707.

11- Y. C. Lv, M. Y. Li, T. Liu, L. J. Tong, T. Peng, L. X. Wei, J. Ding, H. Xie, W. H. Duan, Discovery of a New Series of Naphthamides as Potent VEGFR-2 Kinase Inhibitors, ACS Med. Chem. Lett. 5 (2014) 592.

12- O. Abdel-Rahman, Crit. Rev. Oncol. Hemat. 93 (2015), 18.

13- G. E.-D. A. Abuo-Rahma, M. Abdel-Aziz, E. A. Beshr, T. F. Ali, 1, 2,4-Triazole/oxime hybrids as new strategy for nitric oxide donors: Synthesis, anti-inflammatory, ulceroginicity and antiproliferative activities. Eur. J. Med. Chem 71 (2014) 185-198.

14- P.Ascenzi,A.Bocedi, L.Gradoni, The Anti-Parasitic Effects of Nitric Oxide. IUBMB life 55 (2003) 573-578.

15- B.G. Youssif, M.H. Abdelrahman, A.H. Abdelazeem, H.M. Ibrahim, O.I. Salem, M.F. Mohamed, L. Treambleau, S.N.A. Bukhari, Design, synthesis, mechanistic and histopathological studies of small-molecules of novel indole-2-carboxamides and pyrazino [1, 2-a] indol-1 (2*H*)-ones as potential anticancer agents

effecting the reactive oxygen species production, Eur. J. Med. Chem 146 (2018) 260-273.

16- A.H. Abdelazeem, M.T. El-Saadi, E.G. Said, B.G. Youssif, H.A. Omar, S.M. El-Moghazy, Novel diphenylthiazole derivatives with multi-target mechanism: Synthesis, docking study, anticancer and anti-inflammatory activities, Bioorg. Chem. 75 (2017) 127-138.

17- M.S. Abdelbaset, G.E.-D.A. Abuo-Rahma, M.H. Abdelrahman, M. Ramadan, B.G. Youssif, S.N.A. Bukhari, M.F. Mohamed, M. Abdel-Aziz, Novel pyrrol-2 (3H)-ones and pyridazin-3 (2H)-ones carrying quinoline scaffold as anti-proliferative tubulin polymerization inhibitors, Bioorg. Chem. 80 (2018) 151-163.

18- H.A. El-Sherief, B.G. Youssif, S.N.A. Bukhari, Abdelazeem, A.H.; M. Abdel-Aziz, H.M. Abdel-Rahman. Synthesis, anticancer activity and molecular modeling studies of 1,2,4-triazole derivatives as EGFR inhibitors: Eur. J. Med. Chem 156 (2018) 774-789.

19- M. Hisham, B.G. Youssif, E.E.A. Osman, A.M. Hayallah, M. Abdel-Aziz, Synthesis and biological evaluation of novel xanthine derivatives as potential apoptotic antitumor agents, Eur. J. Med. Chem 176 (2019) 117-128.

20- B.I. Rini, B. Escudier, P. Tomczak, A. Kaprin, C. Szczylik, T.E. Hutson, M.D. Michaelson, V.A. Gorbunova, M.E. Gore, I.G. Rusakov, S. Negrier, Y.-C. Ou, D. Castellano, H.Y. Lim, H. Uemura, J. Tarazi, D. Cella, C. Chen, B. Rosbrook, S. Kim, R.J. Motzer, Comparative effectiveness of axitinib versus sorafenib in advanced renal cell carcinoma (AXIS): a randomised phase 3 trial., Lancet (London, England). 378 (2011) 1931-1939.

21- J.M. Llovet, S. Ricci, V. Mazzaferro, P. Hilgard, E. Gane, J.-F. Blanc, A.C. de Oliveira, A. Santoro, J.-L. Raoul, A. Forner, M. Schwartz, C. Porta, S. Zeuzem, L. Bolondi, T.F. Greten, P.R. Galle, J.-F. Seitz, I. Borbath, D. Haussinger, T. Giannaris, M. Shan, M. Moscovici, D. Voliotis, J. Bruix, Sorafenib in advanced hepatocellular carcinoma., N. Engl. J. Med. 359 (2008) 378–390.

22- M. McTigue, B.W. Murray, J.H. Chen, Y.-L. Deng, J. Solowiej, R.S. Kania, Molecular conformations, interactions, and properties associated with drug efficiency and clinical performance among VEGFR TK inhibitors., Proc. Natl. Acad. Sci. U. S. A. 109 (2012) 18281–18289.

23- K. Okamoto, M. Ikemori-Kawada, A. Jestel, K. von Konig, Y. Funahashi, T. Matsushima, A. Tsuruoka, A. Inoue, J. Matsui, Distinct binding mode of multikinase inhibitor lenvatinib revealed by biochemical characterization, ACS Med. Chem. Lett. 6 (2015) 89-94.

24- D.S. La, J. Belzile, J. V Bready, A. Coxon, T. DeMelfi, N. Doerr, J. Estrada, J.C. Flynn, S.R. Flynn, R.F. Graceffa, S.P. Harriman, J.F. Larrow, A.M. Long, M.W. Martin, M.J. Morrison, V.F. Patel, P.M. Roveto, L. Wang, M.M. Weiss, D.A. Whittington, Y. Teffera, Z. Zhao, A.J. Polverino, J.-C. Harmange, Novel 2,3-dihydro-1,4-benzoxazines as potent and orally bioavailable inhibitors of tumor-driven angiogenesis., J. Med. Chem. 51 (2008) 1695-1705.

25- Dassault systems BIOVIA, Discovery Studio Visualizer, v16.1.0.15350, San Diego: Dassault systems, (2016).

26- R.A. Laskowski, M.B. Swindells, LigPlot+: multiple ligand-protein interaction diagrams for drug discovery, J. Chem. Inf. Model. 51 (2011) 2778–2786.

27- M.A. Zeidan, A.S. Mostafa, R.M. Gomaa, L.A. Abou-Zeid, M. El-Mesery, M.A.-A. El-Sayed, K.B. Selim, Design, synthesis and docking study of novel

picolinamide derivatives as anticancer agents and VEGFR-2 inhibitors., Eur. J. Med. Chem. 168 (2019) 315-329.

28- K. Atwal, B. O'reilly, J.Gougoutas, M. Malley, Synthesis of substituted 1, 2, 3, 4-tetrahydro-6-methyl-2-thioxo-5-pyrimidinecarboxylic acid esters. Heterocycles 26 (1987) 1189-1192.

29- J. Zhang, X. Jiang, Y. Jiang, M. Guo, S. Zhang, J. Li, J. He, J. Liu, J. Wang, L. Ouyang, Recent advances in the development of dual VEGFR and c-Met small molecule inhibitors as anticancer drugs, Eur. J. Med. Chem. 108 (2016) 495-504.

30- K. Holmes, O.L. Roberts, A.M. Thomas, M.J. Cross, Vascular endothelial growth factor receptor-2: Structure, function, intracellular signalling and therapeutic inhibition, Cell. Signal. 19 (2007) 2003-2012.

31- J. Gille, R. Heidenreich, A. Pinter, J. Schmitz, B. Boehme, D.J. Hicklin, R. Henschler, G. Breier, Simultaneous blockade of VEGFR-1 and VEGFR-2 activation is necessary to efficiently inhibit experimental melanoma growth and metastasis formation, Int. J. Cancer 120 (2007) 899-1908.

32- G.M. Morris, R. Huey, W. Lindstrom, M.F. Sanner, R.K. Belew, D.S. Goodsell, A.J. Olson, AutoDock4 and AutoDockTools4: Automated docking with selective receptor flexibility, J. Comput. Chem. 30 (2009) 2785-2791.

33- T.S. Ibrahim, R.M. Bokhtia, A.M.M. AL-Mahmoudy, E.S. Taher, M.A. AlAwadh, M. Elagawany, E.H. Abdel-Aal, S. Panda, A.M. Gouda, H.Z. Asfour, N.A. Alhakamy, B.G.M. Youssif, Design, synthesis and biological evaluation of novel 5-((substituted quinolin-3-yl/1-naphthyl) methylene)-3-substituted imidazolidin-2,4-dione as HIV-1 fusion inhibitors, Bioorg. Chem. 99 (2020) 103782.

34- F.A. Almalki, A.M. Gouda, M.H. Bin Ali, O.M. Almehmadi, Profens: a comparative molecular docking study into cyclooxygenase-1/2, Drug Invent Today 11 (2019) 480-487.

35- A.M. Shawky, M.A.S. Abourehab, A.N. Abdalla, A.M. Gouda, Optimization of pyrrolizine-based Schiff bases with 4-thiazolidinone motif: Design, synthesis and investigation of cytotoxicity and anti-inflammatory potency, Eur. J. Med. Chem. 185 (2020) 111780.

36- M.S. Shaykoon, A.A. Marzouk, O.M. Soltan, A.S. Wanas, M.M. Radwan, A.M. Gouda, B.G.M. Youssif, M. Abdel-Aziz, Design, synthesis and antitrypanosomal activity of heteroaryl-based 1,2,4-triazole and 1,3,4-oxadiazole derivatives, Bioorg. Chem. 100 (2020) 103933.

37- S.A. Rostom, Synthesis and in vitro antitumor evaluation of some indeno [1, 2-c]pyrazol(in)es substituted with sulfonamide, sulfonylurea(thiourea) pharmacophores, and some derived thiazole ring systems, Bioorg. Med. Chem. 14 (2006) 6475-6485.

38- D. Wei, H. Fan, K. Zheng, X. Qin, L. Yang, Y. Yang, Y. Duan, Q. Zhang, C. Zeng, L. Hu**.** Synthesis and anti-tumor activity of [1,4] dioxino [2,3-f] quinazoline derivatives as dual inhibitors of c-Met and VEGFR-2, Bioorg. Chem. 88 (2019) 102916.

[39] B.G.M. Youssif, A.M. Mohamed, E.E.A. Osman, O.F. Abou-Ghadir, D.H. Elnaggar, M.H. Abdelrahman, L. Treamblu, H.A.M. Gomaa, 5-Chlorobenzofuran-2-carboxamides: From allosteric CB1 modulators to potential apoptotic antitumor agents, Eur. J. Med. Chem. 177 (2019) 1–11.

[40] H.A. Abou-Zied, B.G.M. Youssif, M.F.A. Mohamed, A.M. Hayallah, M. Abdel-Aziz, EGFR inhibitors and apoptotic inducers: Design, synthesis, anticancer

activity, and docking studies of novel xanthine derivatives carrying chalcone moiety as hybrid molecules, Bioorg. Chem. 89 (2019) 102997.

Appendix A

4.1. Chemistry

General details

All chemicals used for the preparation of the target compounds are of analytical grade and were purchased from Fluka, Merck, Aldrich and El Nasr pharmaceutical chemicals companies. The reaction progress as well as product purity were monitored using TLC (Kieselgel 60 F254 precoated plates, E. Merck, Dermastadt, Germany), the spots were detected by exposure to UV lamp at λ 254 and 365 nm. Melting points were determined on Stuart electrothermal melting point apparatus and were uncorrected. IR spectra were recorded as KBr disks on SHIMADZU IR-470 spectrophotometer, at the Central Lab, Faculty of Pharmacy, Assiut University or Thermo Scientific Nicolet 380 FT-IR instrument using OMNIC software, Halaweish Lab., South Dakota State University, USA. ^{1}H-NMR spectra were run on Varian Mercury 400 MHz spectrometer, USA. School of Pharmacy University of Mississippi University MS 38677, USA. TMS was used as an internal standard and CDCl3 or

DMSO-*d*6 as a solvent. Chemical shift (δ) values are expressed in parts per million (ppm) and coupling constants (*J*) in Hertz (Hz). The signals are designated as follows: s, singlet; d, doublet; t, triplet; q, quartet; m, multiplet; brs, broad singlet. ^{13}C-NMR spectra were recorded on Varian Mercury 100 MHz spectrometer, USA. School of Pharmacy University of Mississippi University MS 38677, USA. TMS was used as an internal standard and $CDCl_3$ or DMSO-d_6 as solvent. Chemical shift (δ) values are expressed in parts per million (ppm). High resolution mass spectra (HRMS) were obtained on a Thermo Scientific Q Exactive™ Orbitrap mass spectrometer, Faculty of Pharmaceutical sciences, The University of British Columbia, Canada. Elemental analyses were recorded on Perkin Elmer 2400 CHN, The Regional Center for Mycology and Biotechnology, Al-Azhar University.

4.2.1 Evaluation of *in vitro* antiproliferative activity for compounds selected by NCI

The methodology of the NCI anticancer screening has been described in detail elsewhere (http://www.dtp.nci.nih.gov). Briefly, the primary anticancer assay was performed at approximately 60 human tumor cell lines panel derived from nine neoplastic diseases, in accordance with the protocol of the Drug Evaluation Branch, National Cancer Institute, Bethesda, USA. Tested compounds were added to the culture at a single concentration (10^{-5} M) and the cultures were incubated for 48 h. End point determinations were made with a protein binding dye, SRB. Results for each tested compound were reported as the percent of growth of the treated cells when compared to the untreated control cells. The percentage growth was evaluated spectrophotometrically versus controls not treated with test agents. The cytotoxic and/or growth inhibitory effects of the most active selected compound were tested *in vitro* against the full panel of about 60 human tumor cell lines at 10-fold dilutions of

five concentrations ranging from 10^{-4} to 10^{-8} M. A 48-h continuous drug exposure protocol was followed and an SRB protein assay was used to estimate cell viability or growth. Using the seven absorbance measurements [time zero (Tz), control growth in the absence of drug (C), and test growth in the presence of drug at the five concentration levels (Ti)], the percentage growth was calculated at each of the drug concentrations levels. Percentage growth inhibition was calculated as: [(Ti - Tz)/(C - Tz)] × 100 for concentrations for which Ti > Tz, and [(Ti - Tz)/Tz] × 100 for concentrations for which Ti < Tz.

Three-dose response parameters were calculated for each compound. Growth inhibition of 50% (GI_{50}) was calculated from [(Ti - Tz)/(C - Tz)] × 100 = 50, which is the drug concentration resulting in a 50% lower net protein increase in the treated cells (measured by SRB staining) as compared to the net protein increase seen in the control cells. The drug concentration resulting in TGI was calculated from Ti = Tz. The LC_{50} (concentration of drug resulting in a 50% reduction in the measured protein at the end of the drug treatment as compared to that at the beginning) indicating a net loss of cells following treatment was calculated from [(Ti - Tz)/Tz] × 100 = -50. Values were calculated for each of these three parameters if the level of activity is reached; however, if the effect was not reached or was exceeded, the value for that parameter was expressed as more or less than the maximum or minimum concentration tested. The log GI_{50}, log TGI, and log LC_{50} were then determined, defined as the mean of the logs of the individual GI_{50}, TGI, and LC_{50} values. The lowest values are obtained with the most sensitive cell lines. Compound having log GI_{50} values -4 and <-4 was declared to be active.

4.2.2. VEGFR-2 inhibitory assay

The effects of the compounds on VEGFR-2 kinase were determined using enzyme-linked immunosorbent assays (ELISAs) with purified recombinant proteins. Briefly, 20 μg/mL poly (Glu,Tyr) 4:1 (Sigma) was pre-coated in 96-well plates as a substrate. A 50 μL aliquot of 10 μmol/L ATP solution diluted in kinase reaction buffer (50 mmol/L HEPES [pH 7.4], 50 mmol/L $MgCl_2$, 0.5 mmol/L $MnCl_2$, 0.2 mmol/L Na_3VO_4, and 1 mmol/L DTT) was added to each well; 1 μL of various concentrations of indicated compounds diluted in 1% DMSO (v/v) (Sigma) were then added to each reaction well. DMSO (1%, v/v) was used as the negative control. The kinase reaction was initiated by the addition of purified tyrosine kinase proteins diluted in 49 μL of kinase reaction buffer. After incubation for 60 min at 37 ^{0}C, the plate was washed three times with phosphate-buffered saline (PBS) containing 0.1% Tween 20 (T-PBS). Anti-phosphotyrosine (PY99) antibody was then added. After a 30-min incubation at 37 ^{0}C, the plate was washed three times, and horseradish peroxidase-conjugated goat anti-mouse IgG was added. The plate was then incubated at 37 ^{0}C for 30 min and washed 3 times. A 100 μL aliquot of a solution containing 0.03% H_2O_2 and 2 mg/ml *O*-phenylenediamine in 0.1 mol/L citrate buffer (pH 5.5) was added. The reaction was terminated by the addition of 50 μL of 2 mol/L H_2SO_4 as the color changed, and the plate was analyzed using a multi-well spectrophotometer (Spectra MAX 190, Molecular Devices) at 490 nm. The inhibition rate (%) was calculated using the following equation: [1 - (A490/A490 control)] x 100%. The IC_{50} values were calculated from the inhibition curves in two separate experiments.

Cell cycle analysis and apoptosis assay

Cell cycle analysis and apoptosis detection.

Cell cycle analysis was performed for compound **3e** on Leukemia SR cell line. After treatment, the cells were suspended in 0.5 mL of PBS, collected by centrifugation,

and fixed in ice-cold 70% (v/v) ethanol washed with PBS, resuspended with 0.1 mg/mL RNase, stained with 40 mg/ml PI, and analyzed by flow cytometry using FACS caliber (Becton Dickinson). The cell cycle distributions were calculated using Phoenix Flow Systems and Verity Software House

Apoptosis assay

The Leukemia SR was treated with IC_{50} of compound **3e** for 24 h. After treatment, the cells were suspended in 0.5 mL of PBS, collected by centrifugation, and fixed in ice-cold 70% (v/v) ethanol, centrifuged the ethanol-suspended cells for 5 min, suspended in 5 mL PBS and centrifuged for 5 min, re-suspended with 1 mL PI staining solution (0.1 mg/ml RNase) + PE Annexin V (component no. 51-65875X) and kept in dark at 37 ˚C for 10 min, finally analyzed by flow cytometry using FACS caliber (Becton Dickinson). The cell cycle distributions were calculated using Phoenix Flow Systems and Verity Software House.

Design and synthesis of new 1,6-dihydropyrimidin-2-thio derivatives targeting VEGFR-2: molecular docking and antiproliferative evaluation

Adel A. Marzouk[a], Salah A. Abdel-Aziz[a,b], Kamal S. Abdelrahman[a], Amira S. Wanas [c,d], Ahmed M. Gouda[e], Bahaa G. M. Youssif [f], Mohamed Abdel-Aziz [g]

[a]Department of Pharmaceutical Chemistry, Faculty of Pharmacy, Al-Azhar University, Assiut Branch, Assiut-71524, Egypt; [b]Department of Pharmaceutical Chemistry, Faculty of Pharmacy, Deraya University, Minia, Egypt; [c] National Center for Natural

Products Research, University of Mississippi, MS 38677, USA; [d] *Pharmacognosy Department, Faculty of Pharmacy, Minia University, 61519-Minia, Egypt;* [e] *Department of Medicinal Chemistry, Faculty of Pharmacy, Beni-Suef University, Beni-Suef 62514, Egypt;* [f] *Pharmaceutical Organic Chemistry Department, Faculty of Pharmacy, Assiut University, Assiut 71526, Egypt;* [g]*Department of Medicinal Chemistry, Faculty of Pharmacy, Minia University, 61519-Minia, Egypt.*

Conflicts of interest

The authors declare no conflict of interest

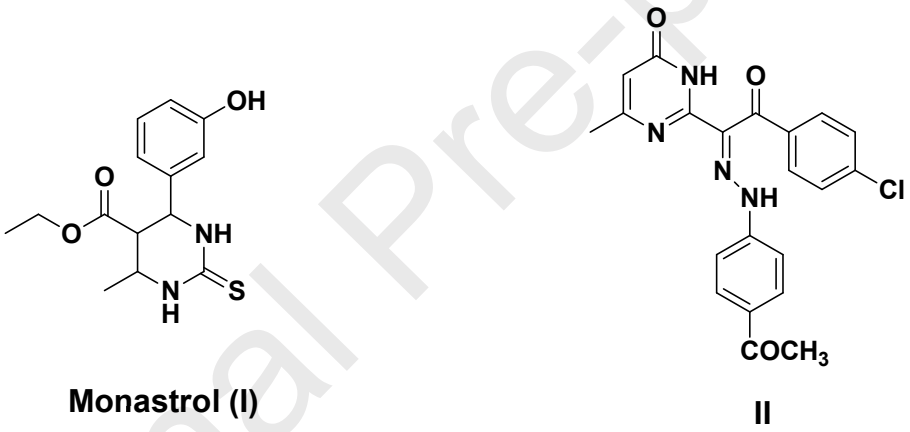

Figure 1: Structure of monastrol **I** and compound **II**

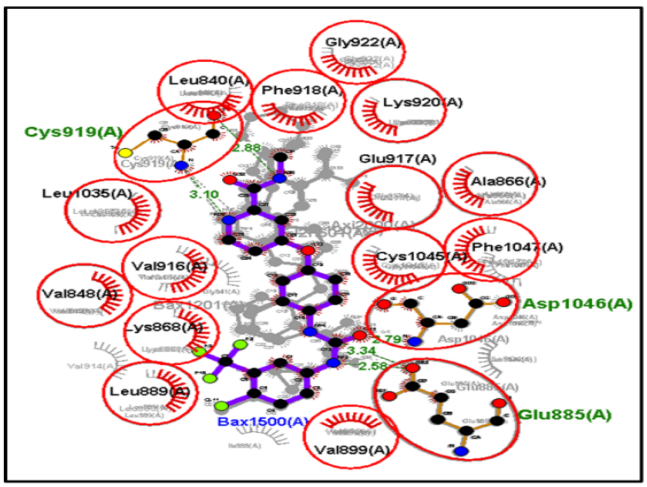

Fig. 2. A superimposition plot of sorafenib, lenvatinib, 2RL, axitinib bound to VEGFR-2 (pdb codes: 4ASD, 4AC, 3WZD, 3WZD, 3WZE, 2RL5), sorafenib is shown in full purple color and is overlaid on lenvatinib, 2RL and axitinib (grey color), red circles and ellipses identify the equivalent residues in the five 3D structures, hydrogen bonding interactions with Lys868, Glu885, Cys919, and Asp1046 shown as olive green dotted line.

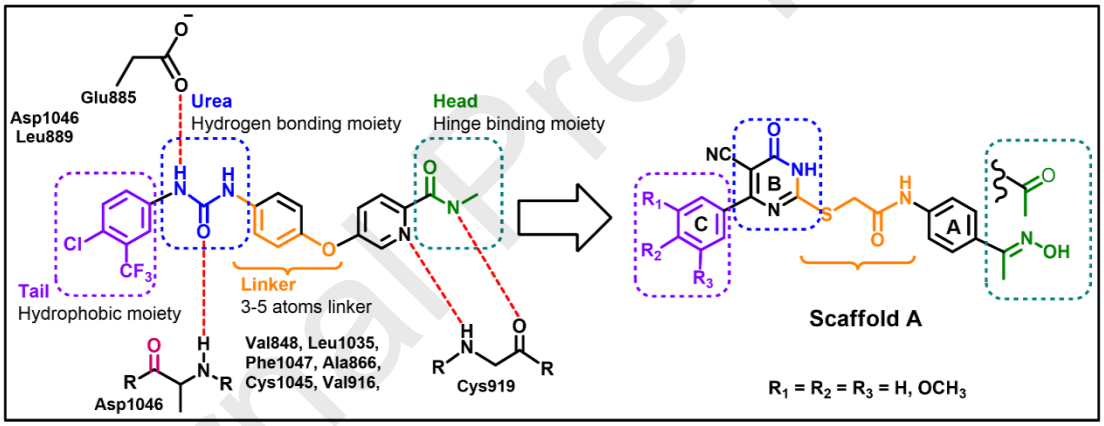

Fig. 3. Rational design of **scaffold A**.

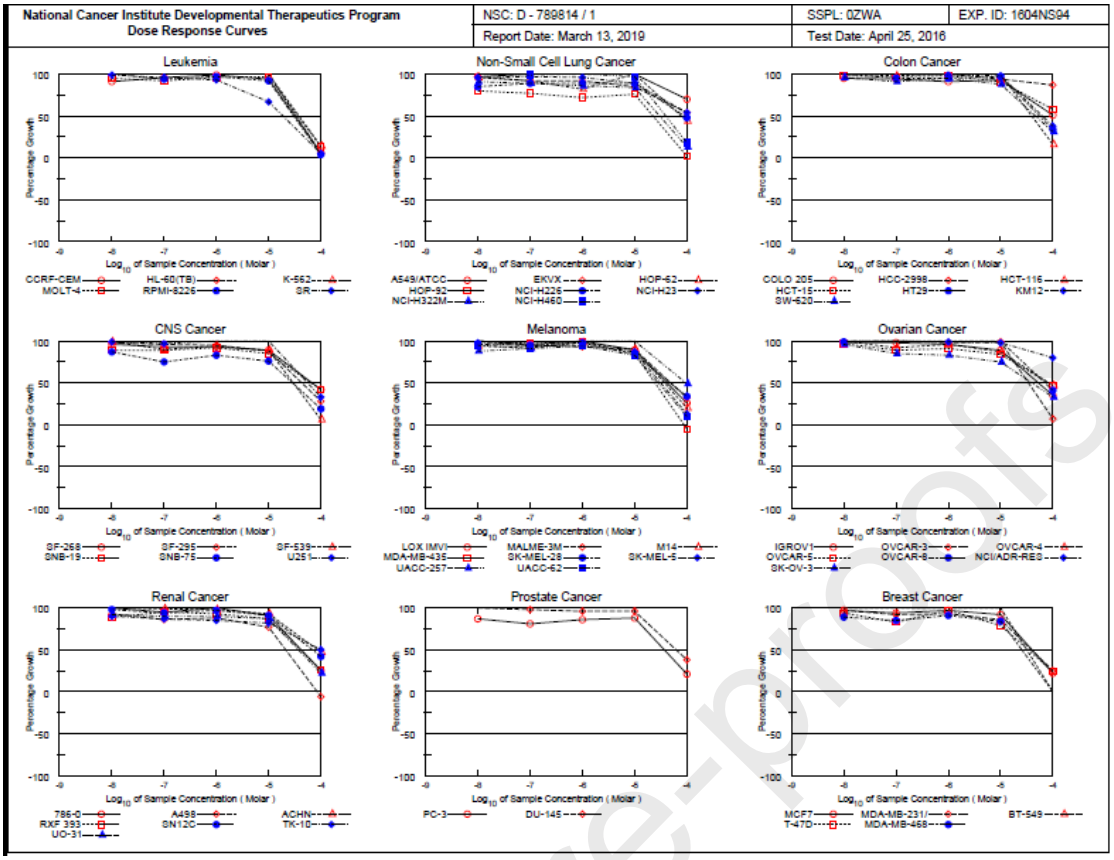

Fig. 4. Dose-antiproliferative response of compound **3e** against nine different cancer cell lines

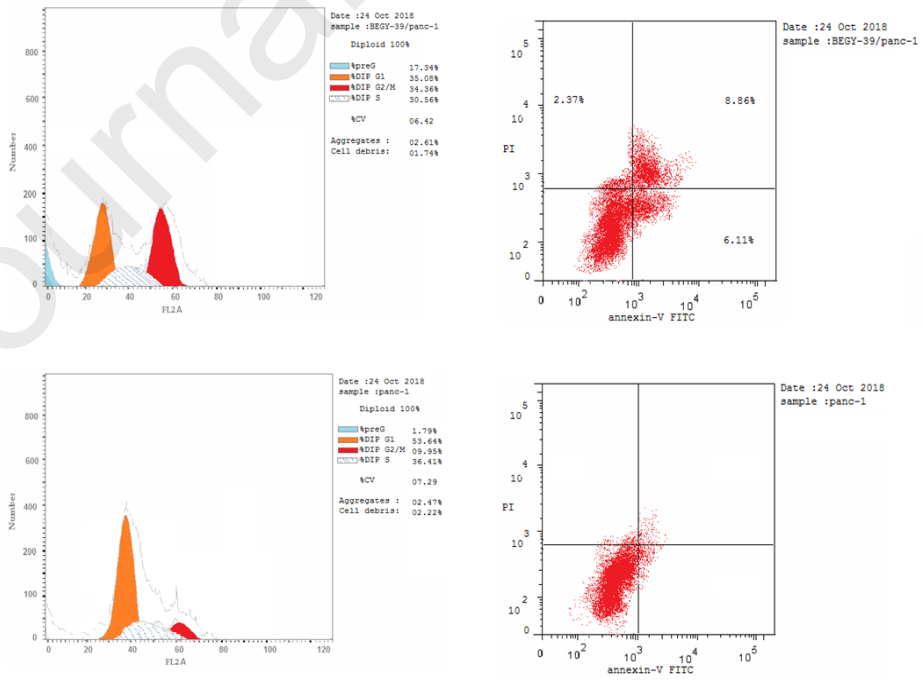

Fig. 5. Cell cycle analysis in Leukemia SR cell line treated with compound **3e**

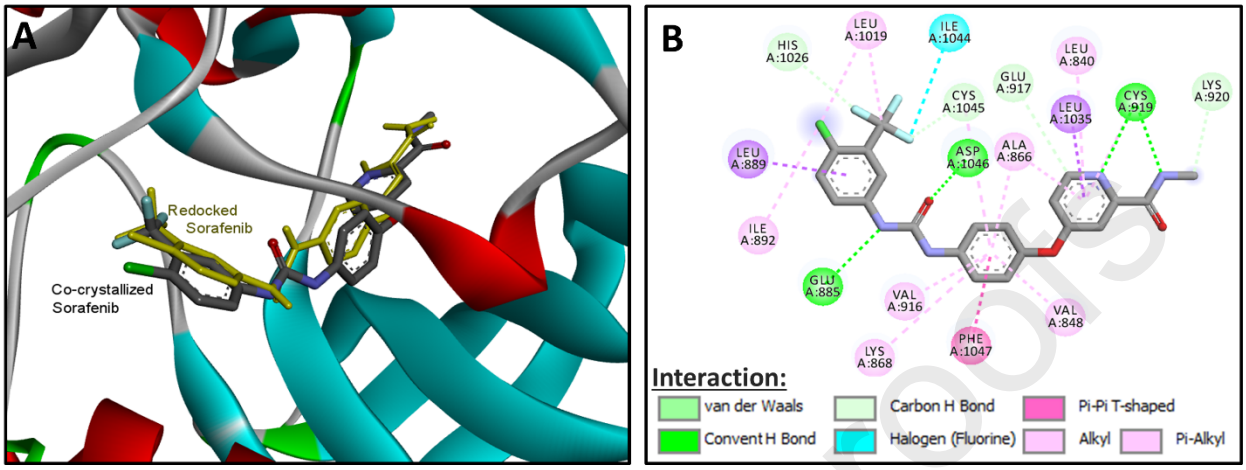

Fig. 6: Binding mode/interactions of redocked/co-crystallized sorafenib into the active of VEFGR-2 (PDB code: 4ASD): A) 3D binding modes showing superimposition of the re-docked ligand (Sorafenib, shown as sticks, colored in yellow) over the native cocrystallized ligand (sorafenib, shown as sticks, colored by element) into the active site of VEGFR-2, RMSD = 1.01 Å; B) 2D binding mode of the re-docked sorafenib into VEGFR-2 showing H-bonding and hydrophobic interactions, hydrogen atoms were omitted for clarity.

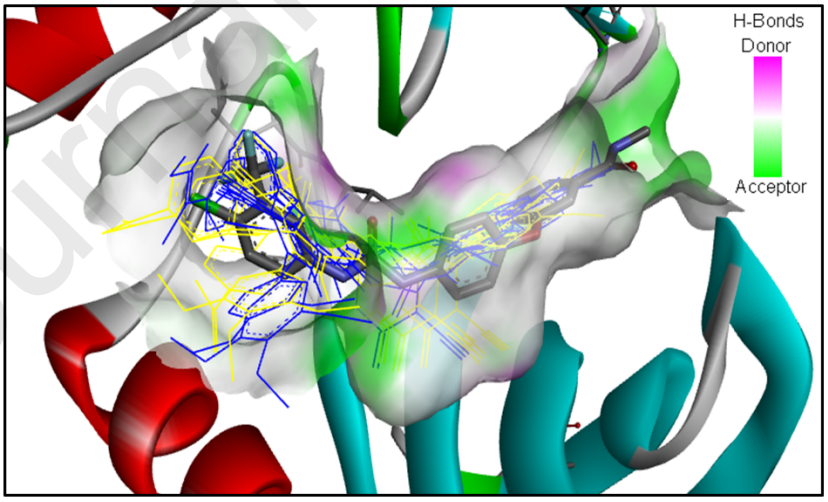

Fig. 7. 3D binding modes of compounds **3a-e** (shown as yellow lines) and compounds **4a-e** (shown as blue lines) overlaid with the native co-recrystallized sorafenib (shown as sticks colored by element) into the active site of VEGFR-2, receptor shown as H-bond surface, hydrogen atoms were hidden for clarity

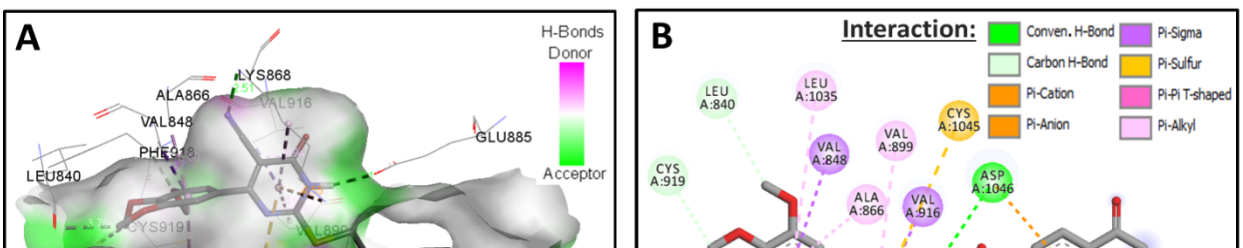

Fig. 8. Binding modes/interactions of compound **3e** into VEGFR (PDB code: 4ASD): A) 3D binding mode of compound **3e** (shown as stick, colored by element), receptor surface shown as H-bond donor (pink) and acceptor (light green); B) 2D binding mode of compound **3e (**shown as stick, colored by element); hydrogen atoms were omitted for clarity.

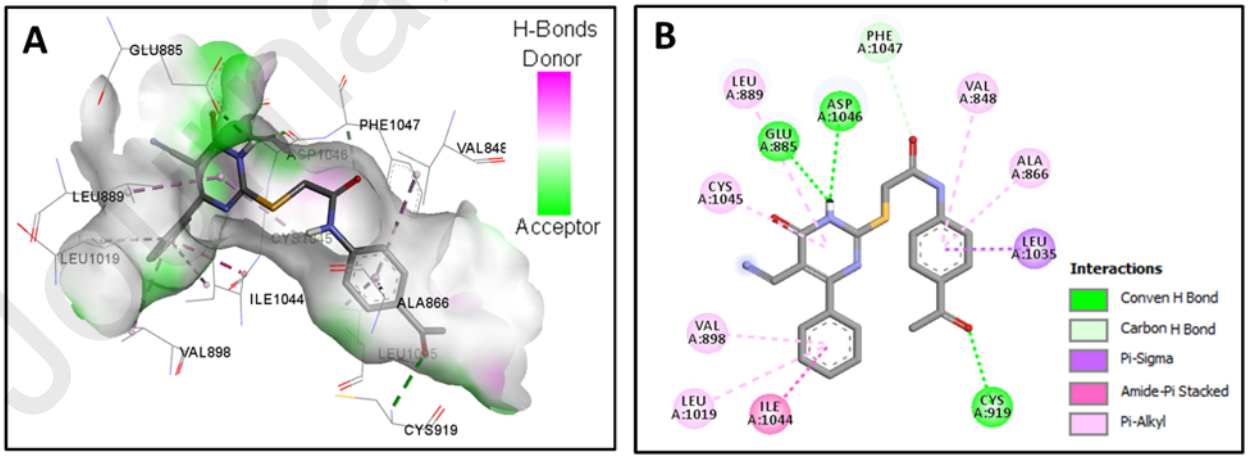

Fig. 9. Binding modes/interactions of compound **3a** into VEGFR(PDB code: 4ASD): A) 3D binding mode of compound 3a (shown as stick, colored by element), receptor surface shown as H-bond donor (pink) and acceptor (light green); B) 2D binding mode of compound **3a (**shown as stick, colored by element); hydrogen atoms were omitted for clarity.

Fig. 10. 3D Binding modes of compound **3b** and **4b** into VEGFR(PDB code: 4ASD): A) 3D binding mode of compound **3b** (shown as stick, colored by element), overlaid with sorafenib (shown as orange line); B) 3D binding mode of compound **4b** (shown as stick, colored by element), overlaid with sorafenib (shown as orange line), receptor shown as H-bond surface.

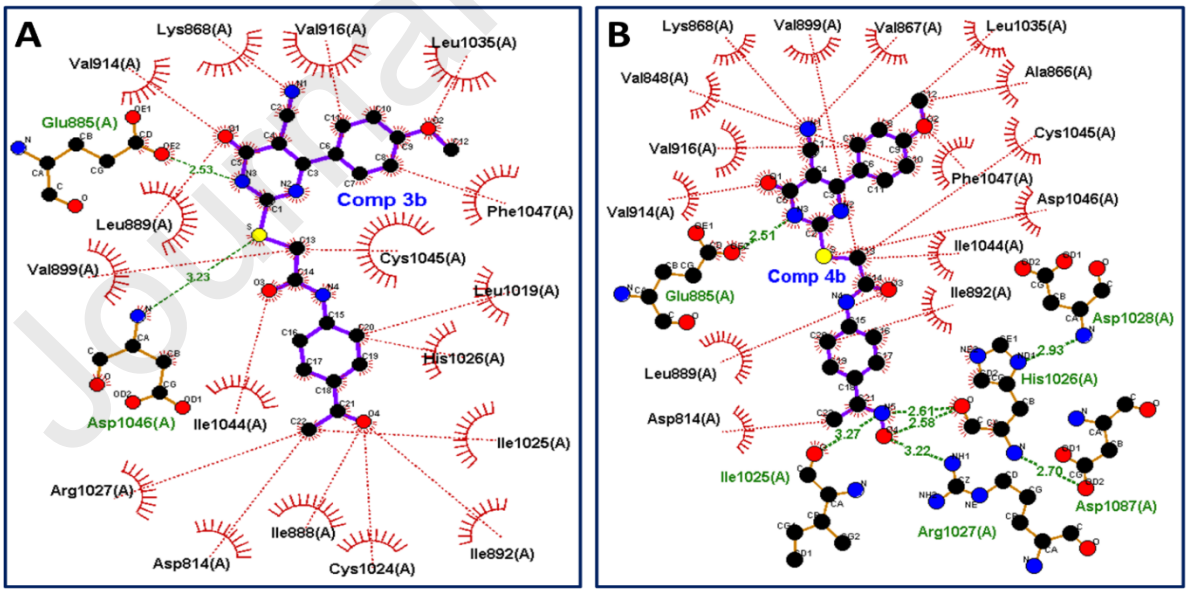

Fig. 11: LigPlot view of compound **3b** and**4b**:A) LigPlot view of compound **3b** into the binding site ofVEGFR-2 (PDB code: 4ASD) showing two conventional hydrogen bonds with Glu885 and Asp1046; B) LigPlot view of compound **4b**into VEGFR-2 showing five hydrogen bonds with Glu885, Ile1025, His1026 and Arg1027;

hydrophobic interactions shown as brick red dotted lines and hydrogen bonding interactions shown as olive green dotted lines.

Graphical abstract

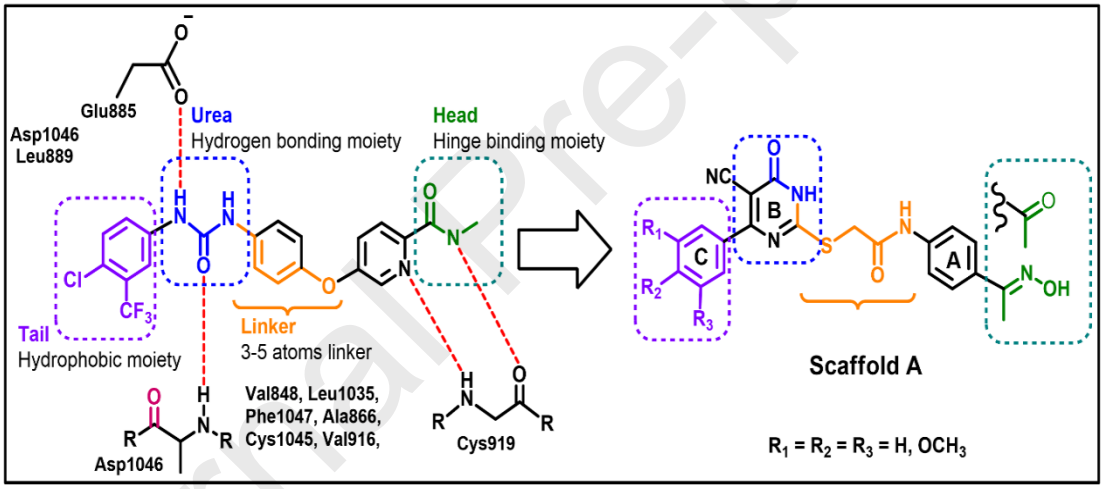

Table 1: Single concentration mean graph growth inhibition of nine different cancer cell types for compounds **3a**, **3b**, **3e** and **4b**

Subpanel cancer cell Lines	% Growth Inhibition (GI %)[a]

	3a	3b	3e	4b
Leukemia				
CCRF-CEM	15.89	-9.5	**111.9**	**-13.0**
HL-60(TB)	51.46	**11.8**	154.3	-6.55
K-562	28.47	1.10	99.46	21.08
MOLT-4	28.72	-3.30	**96.16**	**-5.33**
RPMI-8226	13.93	-14.4	92.53	-12.6
SR	11.31	2.49	**92.38**	9.38
Non-small cell lung cancer				
A549/ATCC	14.01	14.67	80.22	22.97
EKVX	-0.77	-2.14	66.24	-2.49
HOP-62	19.26	-0.94	79.28	14.89
HOP-92	56.20	1.68	89.66	9.50
NCI-H226	5.64	9.04	41.54	13.18
NCI-H23	-2.77	2.83	61.61	8.86
NCI-H322M	-15.6	-0.95	54.71	-7.94
NCI-H460	-10.8	-11.4	94.21	-8.72
NCI-H522	21.22	32.06	114.5	32.95
Colon cancer				
COLO 205	6.12	-14.8	116.2	-14.7
HCC-2998	-14.5	-5.35	78.98	-0.39
HCT-116	37.64	23.71	96.08	20.51
HCT-15	2.31	-3.11	59.78	-9.07
HT29	-4.15	-1.38	93.18	11.69
KM12	-4.62	-1.48	83.25	0.23
SW-620	3.50	-11.9	74.17	-6.13
CNS cancer				
SF-268	-6.20	-0.59	73.15	7.31
SF-295	11.02	4.93	96.6	-1.33
SF-539	5.12	2.36	122.9	9.14
SNB-19	7.65	3.48	41.78	8.92
SNB-75	-12.1	11.73	61.87	9.52
U251	10.88	10.63	83.98	15.65
Melanoma				
LOX IMVI	2.96	3.84	81.51	17.24
MALME-3M	2.84	-2.75	30.49	-1.95
M14	16.40	12.41	94.83	20.6
MDA-MB-435	-0.55	-11.2	146.0	-5.70
SK-MEL-2	-3.79	-3.68	64.11	6.38
SK-MEL-28	1.20	-0.54	42.23	-3.87

SK-MEL-5	3.36	-0.45	84.75	2.13
UACC-257	5.25	15.34	46.34	20.27
UACC-62	4.32	-	64.04	-
Ovarian cancer				
IGROV1	-8.53	-5.76	61.55	-10.0
OVCAR-3	-6.48	-8.04	99.62	-4.14
OVCAR-4	-3.52	-7.54	38.52	2.46
OVCAR-5	-2.74	-2.73	48.11	-8.26
OVCAR-8	6.35	8.97	76.81	14.95
NCI/ADR-RES	-6.05	-8.37	24.3	2.61
SK-OV-3	15.88	20.54	65.44	39.51
Renal cancer				
786-0	11.75	5.27	64.53	-0.11
A498	18.04	1.90	81.52	-7.72
ACHN	-0.61	-0.51	58.41	4.19
CAKI-1	-0.45	3.76	38.45	12.89
RXF 393	-8.64	-7.57	75.44	-3.30
SN12C	-0.11	5.50	70.53	7.12
TK-10	-	1.64	-	12.08
UO-31	7.90	-5.03	50.65	9.64
Prostate cancer				
PC-3	39.38	11.97	81.96	0.88
DU-145	-8.73	-6.43	85.87	-1.04
Breast cancer				
MCF7	20.93	2.55	81.79	8.36
MDA-MB-231/ATCC	-6.88	4.80	80.27	19.80
HS 578T	0.42	-14.8	89.44	3.63
BT-549	20.06	17.77	63.15	14.05
T-47D	22.99	10.55	64.13	41.9
MDA-MB-468	0.83	-5.25	112.8	9.92

Table 2: *In vitro* five dose full NCI 60 cell panel assay of **3e**

Panel	**Cell line**	**GI_{50}**			**TGI**	**LC_{50}**
		Conc. per	**Subpanel**	**Selectivity ratio**	**Conc. per**	

		cell line	MID^b	(MID^a/MID^b)	cell line	
Leukemia	CCRF-CEM	31.60	31.60	1.71	>100	>100
	HL-60(TB)	35.00			>100	>100
	K-562	37.70			>100	>100
	MOLT-4	36.40			>100	>100
	RPMI-8226	29.90			>100	>100
	SR	19.00			>100	>100
Non-small cell lung cancer	A549/ATCC	>100	70.14	0.77	>100	>100
	EKVX	>100			>100	>100
	HOP-62	79.3			>100	>100
	HOP-92	22.60			>100	>100
	NCI-H226	89.80			>100	>100
	NCI-H23	>100			>100	>100
	NCI-H322M	30.30			>100	>100
	NCI-H460	39.10			>100	>100
Colon cancer	COLO 205	>100	72.58	0.75	>100	>100
	HCC-2998	>100			>100	>100
	HCT-116	42.10			>100	>100
	HCT-15	>100			>100	>100
	HT29	55.70			>100	>100
	KM12	63.60			>100	>100
	SW-620	46.70			>100	>100
CNS cancer	SF-268	68.70	48.23	1.12	>100	>100
	SF-295	43.00			>100	>100
	SF-539	29.60			>100	>100
	SNB-19	64.00			>100	>100

	SNB-75	28.50			>100	>100
	U251	55.60			>100	>100
Melanoma	LOX IMVI	41.70	44.54	1.22	>100	>100
	MALME-3M	48.10			>100	>100
	M14	37.40			>100	>100
	MDA-MB-435	24.30			87.60	>100
	SK-MEL-28	47.50			>100	>100
	SK-MEL-5	31.90			>100	>100
	UACC-257	97.40			>100	>100
	UACC-62	28.00			>100	>100
Ovarian cancer	IGROV1	53.40	66.81	0.81	>100	>100
	OVCAR-3	34.00			>100	>100
	OVCAR-4	82.90			>100	>100
	OVCAR-5	85.10			>100	>100
	OVCAR-8	73.70			>100	>100
	NCI/ADR-RES	>100			>100	>100
	SK-OV-3	38.60			>100	>100
Renal cancer	786-0	41.70	55.97	0.968	>100	>100
	A498	21.30			85.00	>100
	ACHN	85.00			>100	>100
	RXF-393	40.10			>100	>100
	SN12C	70.20			>100	>100
	TK-10	96.90			>100	>100
	UO-31	36.60			>100	>100
Prostate cancer	PC-3	36.40	49.5	1.09	>100	>100
	DU-145	62.60			>100	>100

Breast cancer	**MCF7**	**40.00**	**33.94**	**1.60**	**>100**	**>100**
	MDA-MB-231/ATCC	**38.70**			**>100**	**>100**
	BT-549	**32.00**			**99.70**	**>100**
	T-47D	**34.00**			**>100**	**>100**
	MDA-MB-468	**25.40**			**>100**	**>100**
MID[a]			**54.16**			

Table 3: The enzymatic inhibitory activities against VEGFR-2 for compounds **3a**, **3b**, **3e** and **4b**.

Compound	IC_{50} (nμ)
3a	386.4
3b	> 1000
3e	198.7
4b	> 1000
Sorafenib	0.17

Table 4. Apoptosis detection of **3e** in Leukemia SR cancer cell line

Compound	Apoptosis			Necrosis
	Total	Early	Late	
3e / Leukemia SR	17.34	6.11	8.86	2.37
Cont. Leukemia SR	1.79	1.02	0.47	0.3

Highlights

- A series of novel 1,6-dihydropyrimidin-2-thio **(3a-e** and **4a-e)** was designed and synthesized.
- Compounds **3a**, **3b**, **3e** and **4b** were selected for *in vitro* anticancer activity by National Cancer Institute.
- Compound **3e** exhibited a remarkable anticancer activity against most of the cell lines tested.

- *In vitro* five dose assay results showed that **3e** have GI_{50} ranging from 19 to 100 μM with selectivity ratios from 0.75 to 1.71.
- Compounds **3a** and **3e ,** the most potent analogues against VEGFR-2, showed a good fitting to the active site of VEGFR-2.